Duchenne muscular dystrophy is driven by defective membrane repair and annexin-A2 dysregulation in skeletal muscle

Mégane Le Quang[1,2,8*], Léna d'Agata[1*], Romain Carmeille[1], Phoebe Rassinoux[1,3], Joana Ruiz[1], Céline Gounou[1], Antoine Salesses[1], Flora Bouvet[1], Kamel Mamchaoui[4], Sandra Dovero[5], Nathalie Deburgrave[6], France Leturcq[6], Guilhem Solé[7], Marie-Laure Martin-Négrier[2,7,8] and Anthony Bouter[1**]

[1]Univ. Bordeaux, CNRS, Bordeaux INP, CBMN, UMR 5248, F-33600 Pessac, France.

[2]Department of Pathology, University Hospital (CHU) of Bordeaux, Pellegrin Hospital, Place Amélie Raba Léon, 33000, Bordeaux, France.

[3]present address: Institut NeuroMyogène (INMG) - Laboratoire Physiopathologie et Génétique du Neurone et du Muscle, Université Claude Bernard Lyon 1, CNRS UMR 5261, INSERM U1315, Lyon, France.

[4]Sorbonne Université, Inserm, Institut de Myologie, Centre de Recherche en Myologie, F-75013, Paris, France.

[5]Univ. Bordeaux, CNRS, HistoCARE Facility, IMN, UMR 5293, Bordeaux, France.

[6]Service de Medecine Genomique, Maladies de Systeme et d'Organe-Federation de Genetique et de Medecine Genomique, DMU BioPhyGen, APHP Centre-Universite Paris Cite-Hopital Cochin, Paris, France.

[7]Centre de Référence des Maladies Neuromusculaires AOC, Service de Neurologie et Maladies Neuromusculaires, FILNEMUS, EURONMD, Hôpital Pellegrin, CHU de Bordeaux, France.

[8]Univ. Bordeaux, CNRS, IMN, UMR 5293, Bordeaux, France.

*Contribute equally to this work

**Corresponding author, e-mail: anthony.bouter@u-bordeaux.fr; phone: +33 540006860

Running title: Membrane repair and annexins in DMD

ABSTRACT

Background:

Duchenne muscular dystrophy (DMD) is caused by mutations in the *DMD* gene, which encodes dystrophin in skeletal muscle cells. Although the role of dystrophin as a structural protein is well known, the cellular processes underlying myofiber degeneration are still not fully understood. Despite advances from studies in murine models, these models do not fully replicate the human pathology.

Methods:

We investigated sarcolemmal integrity, membrane repair capacity, and annexin protein expression in DMD patient muscle biopsies and human skeletal muscle cell lines using immunohistochemistry, both shear stress-based and laser irradiation injury assays, western blotting, and live-cell imaging of GFP-tagged annexins.

Results:

We identified defective membrane repair in DMD skeletal muscle cells, independent of increased membrane fragility, by evaluating resealing capacity in control and DMD derived-patient cell lines using both a shear stress assay ($N = 12$, $p < 0.0001$) and a laser irradiation assay ($N = 3$, $p < 0.0001$). Analyses performed on human DMD muscle biopsies ($N = 10$) further confirmed this defect, demonstrating massive intracellular IgG uptake ($p < 0.0001$) together with altered annexin expression profiles. While mechanical stress induces the upregulation of annexin A5 (ANXA5, $p < 0.01$) and A6 (ANXA6, $p < 0.05$) in healthy skeletal muscle cells - suggesting an adaptive response to membrane damage, given the annexin family's central role in membrane repair - we observed dysregulated expression patterns of these proteins in DMD cells. Notably, ANXA1 ($p < 0.05$) and ANXA2 ($p < 0.01$) were not only significantly overexpressed but also aberrantly localized to the extracellular space, a putative consequence of defective membrane repair. Since extracellular ANXA2 has been associated with adipocyte accumulation in the muscle tissue of patients with dysferlinopathy, a similar pathological mechanism may be at play in DMD.

Conclusions:

Our findings propose that ANXA2 contributes to muscle degeneration in DMD and highlight it as a potential therapeutic target to prevent adipogenesis and muscle loss.

Keywords: Duchenne muscular dystrophy, membrane repair, annexin, ANXA2, skeletal muscle

Abreviation: ANXA2: Annexin-A2; DMD: Duchenne muscular dystrophy; FAP: fibro-adipogenic progenitors; IgG: immunoglobulin type G; MD: muscular dystrophies; PI: propidium iodide.

1. Introduction

Skeletal muscle fibers are subjected to constant mechanical stress due to contraction, stretching, and shearing forces, which can result in transient disruptions of the sarcolemma [1]. Efficient membrane repair is essential to preserve myofiber viability, and defects in this process contribute to the progression of degenerative muscle diseases, including muscular dystrophies (MDs). Limb-girdle muscular dystrophy type 2B (LGMD2B), now classified as LGMDR2, is a prototypical example of a membrane repair disorder. Caused by mutations in the *DYSF* gene encoding dysferlin, LGMD2B is characterized by defective sarcolemmal resealing, leading to myofiber necrosis and muscle wasting [2]. Notably, annexin-A2 (ANXA2), a calcium-dependent phospholipid-binding protein involved in membrane repair, is upregulated in LGMD2B muscle possibly as a compensatory response to membrane fragility [3,4]. However, persistent sarcolemmal damage results in leakage of intracellular contents, triggering proliferation of fibro-adipogenic progenitors (FAPs) and infiltration of macrophages [5,6]. In murine models, extracellular ANXA2 has been shown to promote adipogenic differentiation of FAPs, contributing to fatty replacement of muscle fibers [3].

Duchenne muscular dystrophy (DMD) is an X-linked disorder caused by mutations in the *DMD* gene, resulting in the loss of dystrophin, which is a structural protein that anchors the actin cytoskeleton to the extracellular matrix via the dystrophin-glycoprotein complex (DGC) [7,8]. Dystrophin deficiency destabilizes the sarcolemma, increasing susceptibility to damage during contraction and disrupting DGC-associated signaling pathways [9,10]. Moreover, disruptions in the DGC complex affect the distribution of associated proteins, further exacerbating the loss of muscle function [11]. Although sarcolemmal fragility in the *mdx* mouse model of DMD has been linked to impaired mitochondrial function and defective membrane repair [12], species-specific differences raise uncertainty about the relevance of these findings to human disease [13].

Here, we investigate membrane repair capacity in human DMD muscle using muscular biopsies and patient-derived skeletal muscle cell lines. We show that DMD myofibers exhibit defective membrane resealing, as evidenced *in vivo* by increased intracellular accumulation of IgG in myofibers with a necrotic outcome and impaired membrane resealing following mechanical stress or laser irradiation *in vitro*. We further identify dysregulation of multiple annexins with ANXA2 significantly overexpressed and mislocalized to the extracellular space in DMD muscle. This pattern mirrors the annexin pathology observed in LGMD2B and correlates with adipocyte accumulation, implicating ANXA2 misregulation as a potential driver of fibro-adipogenic remodeling in DMD.

2. Methods

2.1. Patient Biopsies

Frozen muscle biopsies from 10 DMD patients with confirmed mutations were obtained from the bio-bank of Bordeaux University Hospital (COLMYONEU, Table S1 and S2). As a control, 10 frozen muscle biopsies performed for chronic muscle pain or weakness without characterized neuromuscular conditions, elevated creatine kinase levels and histopathological anomalies were used (Table S3). Informed consents have been obtained from all patients and the study was approved by the Ethics Committee of Bordeaux University Hospital (CER-BDX 2025-214).

2.2. Immortalized Patient-Derived Skeletal Muscle Cells

Human-derived skeletal muscle cell lines were obtained from the Center of myology (UMRS974, Paris, France). Healthy, LGMD2B and DMD patient-derived skeletal muscle cell lines were immortalized with CDK4 and Telomerase-expressing pBABE retroviral vectors as described previously [14]. The immortalized DMD muscle cell lines tested were AB1098 and 6594 [15], herein referred as to DMD1 and DMD2, respectively. Both DMD cell lines present deletions of DMD exons 48–50 leading to the absence of the expression of dystrophin [15,16]. The immortalized healthy muscle cell lines LHCN-M2 and KM1421 were used as controls, herein referred as to CTL1 and CTL2, respectively. We used also the LGMD2B muscle cell line 578 as a positive control, since LGMD2B is associated with a defect in membrane repair [2,14,17]. Cell culture media and reagents were from ThermoFisher Scientific (Waltham, MA, USA) except when otherwise stated. Myoblasts were cultured in a skeletal muscle medium composed by one volume of Medium 199 with glutaMAX™ (Gibco® by Thermo Fisher Scientific, Waltham, MA, USA), four volumes of Dubelcco's modified Eagle Medium (DMEM) with high-glucose and glutaMAX™ and without pyruvate (Gibco® by Thermo Fisher Scientific, Waltham, MA, USA) supplemented with 20% fetal bovine serum, 50 µg/mL gentamycin and a commercial mix of skeletal muscle cell growth medium supplements (Promocell, Heidelberg, Germany), which included 12.5 g/mL fetuin, 2.5 ng/mL human recombinant epidermal growth factor, 0.25 ng/mL basic fibroblast growth factor, 2.5 µg/mL insulin, 0.1 µg/mL dexamethasone. The 24h-differentiated myoblasts and myotubes were obtained by cultivating 90%-confluence myoblasts respectively for one and three days in a differentiation medium, composed of the skeletal muscle medium supplemented only with 10 µg/mL insulin.

2.3. Membrane repair assay by laser irradiation

Membrane repair assay was performed as previously described [17,18]. Myotubes were irradiated at 820 nm with a tunable pulsed depletion laser Mai Tai HP (Spectra-Physics, Irvine, USA) of a two-photon

confocal scanning microscope (TCS SP5, Leica, Wetzlar, Germany). Irradiation consisted of 1 scan (1.6 s) of a 1 µm x 1 µm area with a power of 110 (±5) mW. 512 x 512 images were acquired at 1.6 s intervals with pinhole set to 1 Airy unit. FM1-43 was excited by the 488-nm laser line (intensity set at 20% of maximal power) and fluorescence emission was measured between 520 nm and 650 nm. For quantitative analysis, the fluorescence intensity was integrated over the whole cell surface and corrected for the fluorescence value recorded before irradiation, using ImageJ software.

2.4. Muscle Shear Stress Assay

Experiments were performed as previously described [19]. Differentiated myoblasts for 24 hours, at a concentration of 5×10^5 cells/mL, were divided into two populations: the stressed population was passed ten times through a 30G needle, while the untreated population remained in resting conditions and served as a control. To assess membrane repair, 50 µL of each population were incubated with a mixture of Hoechst (20 µg/mL, Sigma-Aldrich) and PI (2 µg/mL, Sigma-Aldrich) ten minutes after the treatment. To assess membrane fragility, the experiment was performed with cells suspended in 1 mL of growth medium supplemented with 2 mM EGTA, 2 µg/mL PI, and 20 µg/mL Hoechst. PI-positive (damaged, unrepaired) and Hoechst-positive (total) cells were counted by fluorescence microscopy (IX81, Olympus).

2.5. Effect of Shear Stress on Survival Rate and ANX Expression

To assess survival rate, cells were seeded in growth conditions after submitted to the muscle shear stress assay and counted 24 hours later. The survival rate was calculated as the ratio of living cells at 24h to number of seeded cells. To overcome mortality related to experimental conditions (room temperature and atmospheric CO_2), common to both the unstressed and stressed populations, live cell concentration within the untreated population 24 hours after the experiment was measured and the mortality rate due to experimental conditions was calculated. This correction factor was applied to cells subjected to shear stress. Secondly, a significant loss of 10-20% of cell suspension was observed during the shear stress treatment, mainly due to dead volume in the needle-syringe system. To eliminate this bias, the volume of cell suspension seeded after shear stress was systematically measured and all data were proportionally corrected for this loss. We then determined the survival rate by calculating the ratio of the number of surviving cells in the stressed condition to the number of surviving cells in resting condition. The impact of mechanical stress on ANX expression was analyzed by western blot, by comparing expression between stressed and non-stressed cells 24 hours after shear stress.

2.6. Immunohistochemical Analysis of Muscle Sections

Immunofluorescence was performed on 8-µm frozen cross-sections. Blocking was done with 3% BSA and 3% NGS. Primary and secondary antibodies were incubated with NGS 3% respectively at 4°C overnight and at room temperature 2 h. The following primary antibodies were used: rabbit polyclonal anti-ANXA1 (1:100, Boster, PA1006), mouse monoclonal anti-ANXA2 (1:1000, Sigma-Aldrich, WH0000302M1), mouse monoclonal anti-ANXA5 (1:500, Abcam, AB54775), mouse monoclonal anti-ANXA6 (1:500, Santa Cruz, sc-271859), mouse monoclonal anti-MHCf (1:100, Novocastra, WB-MHCf), mouse monoclonal anti-perilipin (1:100, Santa-Cruz, sc-390169) and rabbit polyclonal anti-IgG conjugate with FITC (1:50, Dako Agilent, F0202). Co-labeling with rat monoclonal anti-Laminin α-2 (1:1000, Santa Cruz, sc-59854) or rabbit polyclonal anti-Laminin (1:1000, ThermoFisher, PA116730) was made. Staining was visualized using relevant secondary antibodies conjugated to AlexaFluor 488 or 568 (1:500, Invitrogen). Nuclear counterstaining was performed with 20 µg/mL Hoechst 33342 (Sigma-Aldrich). All slides were digitized using a high-resolution slide scanner (Panoramic Scan II, 3DHISTECH Ltd, France) at x20 magnification. Quantification of the biopsies was performed using ImageJ software. The IgG-positive area was calculated by applying thresholding to exclude non-specific staining and by measuring the total positive area (excluding any epi- or perimysium staining) relative to the entire muscle cross-section. The number of positive fibers was determined by thresholding the image to exclude non-specific staining.

2.7. Western Blot

For muscle cell lines, 2×10^6 cells were trypsinized, pelleted and re-suspended in 300 µL of D-PBS supplemented with 1 mM EGTA. Protein extracts were obtained by sonicating ice-cold cell suspension with a Branson digital sonifier (amplitude 20%, duration 2 min, interval 5 s and pulse 5 s) and their concentration was measured using the Bradford protein assay (Bio-Rad, Hercules, CA, USA). Two successive centrifugations at 8000g for 1 min allowed to remove cell debris. 10 µg protein extracts, together with the Dual color molecular weight marker (Biorad) were separated on a 10% SDS-PAGE. Transfer onto PVDF membrane was performed for 1 h at 100 V. In addition to the antibodies described in the immunohistochemical analysis section, the following primary antibodies were used: anti-dysferlin mouse monoclonal antibody (NCL-Hamlet, Novocastra, 1:250) and anti-dystrophin mouse monoclonal antibody (NCL-DYS1, Novocastra, 1:50). Unless otherwise specified, primary antibodies were used at a 1:1000 dilution in blocking solution. GAPDH was detected with a rabbit anti-GAPDH polyclonal antibody (Santa Cruz Biotechnology) diluted 1:20000, as a loading control. Revelation was performed using secondary antibodies conjugated to horse-radish peroxidase (GE-Healthcare,

Chicago, IL, USA) diluted 1:2000 in saturation solution and Opti-4CN™ colorimetric kit (Bio-Rad, Hercules, CA, USA).

For biopsy analysis, 8-µm frozen sections were homogenized with a lysis buffer containing 2% glycerol, 2% SDS, and 0.125 mol/L Tris-HCL pH 6.4 during 30 min before sonication for 10 min in ice-cold cell suspension. Lysates were stored at -20°C and used within a week. Protein concentration was measured using BCA assessment (BCA1, Sigma-Aldrich). Western blots were performed with 10-20 µg protein extracts separated on SDS-PAGE using stain-free 10% acrylamide gel (Biorad, TGX Stain-Free™ FastCast™ Acrylamide Kit, 10%) and the Precision Plus Protein All Blue Standards (Bio-Rad). Electrophoretic transfer onto PVDF membrane was performed with the Trans-Blot Turbo Transfer System (BioRad) during 7 min at 1.3A/25V. Total protein signals were measured using the Chemi-Doc imager (Bio-Rad) and ImageLab software. Revelation was performed by chemiluminescence using secondary antibodies conjugated to horse-radish peroxidase (GE-Healthcare, Chicago, IL, USA) diluted 1:2000 in saturation solution and Clarity™ Western ECL substrate (Bio-Rad). Dystrophin and dysferlin were respectively detected using the mouse monoclonal NCL-DYS1 and NCL-DYS2 antibodies (Novocastra, 1:50) and NCL-Hamlet monoclonal antibody (Novocastra, 1:250). Annexins were detected with the same antibodies as for immunofluorescence diluted 1:1000 in saturation solution composed by Tris buffer saline (10 mM Tris, 150 mM NaCl, pH 8.0) supplemented with 0.1% Tween20 and 5% non-fat dry milk. ImageLab software was used to measure the relative intensity of protein bands. The Western blot analyses for dysferlin and dystrophin were performed using protocols distinct from those outlined above; the exact methods are provided in the legends of Figures S2 and S7.

2.8. Subcellular Trafficking of ANXA2 Fused to Fluorescent Proteins in Damaged Skeletal Muscle Cells

Sketelal muscle cells expressing the ANXA2-GFP fusion protein were obtained as previously described [20]. Membrane damage was performed on myoblasts differentiated 24h by laser ablation, as previously described [19]. Briefly, myoblasts were cultured and differentiated in a 35-mm glass bottom dish equipped with a square-patterned coverslip (MatTek, Ashland, MA, USA). To induce membrane damage, cells were irradiated at 820 nm with a tunable pulsed depletion laser Mai Tai HP (Spectra Physics, Irvine, USA) of an upright two-photon confocal scanning microscope (TCS SP5, Leica, Wetzlar, Germany) equipped with an HCX APO L U-V-I 63.0 0.90 water lens. Irradiation consisted of 1 scan (1.6 s) of a 1 µm x 1 µm area with a power of 110 (± 5) mW. Images of 512 x 512 were acquired at 1.6 s intervals with pinhole set to 1 Airy unit. At least three independent experiments were performed for each cell type.

2.9. Statistics

Data are presented as mean values (±SEM) from at least three independent experiments performed in triplicate. The statistical significance of data was assessed by a Mann–Whitney or Wilcoxon test using GraphPad Prism software**.** A probability value less than 0.05 is used for statistical significance. *$p < 0.05$, **$p < 0.01$, ***$p < 0.001$, ****$p < 0.0001$.

3. Results

3.1. Human DMD Muscle Cells Suffer from a Defect in Membrane Repair

To assess whether membrane repair is impaired in DMD skeletal muscle cells, we analyzed sarcolemmal integrity in patient biopsies using immunostaining for intracellular IgG uptake, a well-established marker of membrane permeability [21]. Compared to control, DMD muscle exhibited extensive IgG accumulation both within the interstitial space and intracellularly in a substantial proportion of myofibers (**Figure 1**). This indicates widespread membrane damage and the consequent entry of serum IgG into muscle fibers due to loss of membrane integrity, likely resulting from chronic and repeated mechanical stress. Notably, IgG labeling within DMD biopsies was spatially heterogeneous, with discrete regions displaying high or low signal intensity (**Figure S1A**), suggesting local variation in mechanical vulnerability or disease progression. The presence of IgG at comparable levels in both type I and II myofibers indicates that susceptibility to membrane damage is not fiber-type specific in DMD muscle **(Figure S1B).** Collectively, these findings demonstrate frequent and regionally variable disruption of membrane integrity in DMD skeletal muscle. To investigate whether DMD skeletal muscle cells exhibit defective membrane repair, we subjected two patient-derived skeletal muscle cell lines to a recently established shear stress assay [19]. This assay involves passing 24-hour–differentiated myoblasts through a fine-gauge needle, inducing mechanical membrane disruption. We previously demonstrated that at this stage of differentiation, healthy myoblasts possess a functional, Ca^{2+}-dependent membrane repair machinery capable of resealing shear-induced damage [19]. Moreover, we observed that dystrophin is expressed similarly in control undifferentiated and 24-hour–differentiated myoblasts **(Figure S2).** Notably, dystrophin expression increased approximately twofold in myotubes compared to myoblasts **(Figure S2).** In contrast, we confirmed that dystrophin was completely absent from DMD myoblasts and myotubes. For the shear stress assay, DMD myoblasts were analyzed alongside two control cell lines and a positive pathological control cell line derived from a patient with LGMD2B, a muscular dystrophy caused by impaired membrane repair [2]. In the presence of extracellular Ca^{2+}, control cells showed low levels of unrepaired membrane damage, respectively 2.5 ± 1.8% (CTL1) and 2.7 ± 0.9% (CTL2) (**Figure 2B**). By contrast, LGMD2B myoblasts exhibited a significantly higher rate of damage (8.2 ± 2.1%), consistent with a known repair defect (**Figure 2B**). DMD myoblasts displayed similarly elevated levels of unrepaired membrane disruption - 8.1 ± 2.1% (DMD1) and 6.4 ± 1.1% (DMD2) - suggesting a comparable defect in membrane resealing. Because dystrophin is essential for maintaining sarcolemmal stability, the increased damage observed in DMD cells could reflect either defective repair or heightened membrane fragility. To distinguish between both possibilities, we repeated the assay in the absence of Ca^{2+}, a condition that abolishes repair,

allowing assessment of intrinsic membrane susceptibility to shear-induced rupture. Under these conditions, about 20% of control, DMD, and LGMD2B cells exhibited membrane disruption with no significant differences (**Figure 2C**), indicating comparable baseline fragility. Together, these findings demonstrate that the elevated level of unrepaired cells observed in DMD myoblasts under permissive (Ca^{2+}) conditions results from impaired membrane repair capacity rather than increased membrane fragility. Finally, to confirm that DMD muscle cells exhibit a defect in membrane repair, we performed a standard membrane repair assay using laser irradiation on differentiated myotubes in the presence of Ca^{2+} and FM1-43 [17,18]. Following laser-induced injury, FM1-43 enters the cytosol and fluoresces upon incorporation into intracellular membranes. The fluorescence intensity increases until the plasma membrane reseals. In control myotubes, FM1-43 rapidly entered the cell at the site of irradiation within seconds of laser injury, confirming membrane rupture **(Figure 2D, +1.6 s, arrow).** After 120 seconds, most damaged control myotubes displayed fluorescence confined to the region surrounding the disruption site **(Figure 2D, +120 s, arrow).** The fluorescence kinetics revealed that intracellular fluorescence intensity rose for a few tens of seconds before reaching a plateau **(Figure 2E, CTL1, filled circles),** indicating rapid sarcolemmal resealing, as previously reported [17]. In contrast, irradiation of DMD1 or DMD2 myotubes resulted in a markedly greater increase in fluorescence intensity **(Figure 2E, empty circles and triangles),** indicating a failure of membrane resealing. Collectively, these results confirm that the membrane repair process is impaired in DMD muscle cells.

To further assess the functional consequences of impaired membrane repair in DMD cells, we evaluated cell survival 24 hours after exposure to mechanical injury. Control and DMD 24-hour–differentiated myoblasts were subjected to the shear stress assay and subsequently replated in growth medium. After 24 hours, cell viability was quantified. Cell survival following mechanical stress was quantified by comparing the number of viable cells 24 hours post-shear stress to untreated controls. Control myoblasts exhibited near-complete survival, indicating that shear stress did not compromise long-term viability in cells with intact membrane repair capacity (**Figure S3**). In contrast, DMD-derived myoblasts showed significantly reduced survival rates, at respectively 59.6 ± 18.3% (DMD1) and 60.7 ± 14.0% (DMD2), demonstrating that mechanical stress induces substantial cell death in the absence of efficient membrane repair. Interestingly, the observed mortality rates exceeded the proportion of unrepaired cells detected immediately after shear stress (**see Figure 2B**), suggesting that some cells, although initially capable of resealing, may have incurred sublethal damage that compromised survival over time. Alternatively, delayed cell death may occur in cells that withstood initial membrane rupture but failed to recover from mechanical injury. Together, these findings support the conclusion that defective membrane repair in DMD myoblasts leads to delayed cell death following mechanical

challenge. *In vivo*, such a defect likely contributes to progressive muscle fiber necrosis and the pathological release of intracellular components into the extracellular space.

3.2. Annexin Expression is Dysregulated in DMD Muscle Cells

In LGMD2B, impaired membrane repair is accompanied by dysregulation of annexin family members, notably ANXA1 and ANXA2, which may exacerbate disease progression by interfering with repair pathways or amplifying inflammatory signaling [4,22–24]. To investigate whether a similar pattern occurs in DMD, we analyzed the expression of ANXA1, ANXA2, ANXA5, and ANXA6, which are key components of the membrane repair machinery, by western blotting in both human skeletal muscle cell lines and patient biopsies. We first compared annexin expression profiles in muscle biopsies from control individuals and DMD patients (**Figure 3**). As expected, western blot analysis revealed single bands corresponding to the predicted molecular weights of ANXA1 (37 kDa), ANXA2 (36 kDa), ANXA5 (35 kDa), and ANXA6 (68 kDa) (**Figure 3A and Figure S4A**). Previous studies in dysferlin-deficient mice have identified a truncated ANXA6 isoform that impairs membrane localization of the full-length protein [25,26]. Despite extensive efforts, we did not detect any truncated ANXA6 species in human control or DMD muscle biopsies (**Figure 3A and Figure S4A**), suggesting that this isoform may be specific to murine and/or dysferlinopathic skeletal muscle. Quantitative analysis showed that ANXA5 levels were comparable between DMD and control biopsies (**Figure 3B and Figure S4B**). ANXA6 expression was moderately but significantly elevated in DMD samples, with an average twofold increase. In contrast, ANXA1 and ANXA2 were markedly overexpressed in DMD muscle, with fold changes of **8.3 and 9.6**, respectively (**Figure 3B and Figure S4B**). These findings are consistent with previous reports of ANXA1 and ANXA2 upregulation in DMD patient cohorts and in mdx mice [4,12], and confirm their dysregulation in human DMD muscle. In summary, while ANXA5 and ANXA6 expression is minimally altered, ANXA1 and ANXA2 are strongly upregulated in DMD skeletal muscle tissue. To extend our analysis, we examined annexin expression in myotubes derived from control and DMD patient cell lines differentiated for three days (**Figure 4A and Figure S5**). ANXA5 and ANXA6 were detected as single bands at their expected molecular weights of 35 kDa and 68 kDa, respectively. In contrast, ANXA1 and ANXA2 appeared as multiple bands - up to three - likely reflecting proteolytic processing, as previously reported for ANXA2 [27,28]. To quantify overall protein abundance, all bands corresponding to a given annexin were summed, and data from the two control and two DMD cell lines were pooled to improve statistical robustness (**Figure 4B**). No significant differences were observed in ANXA5 or ANXA6 expression between control and DMD myotubes. A modest increase in ANXA1 expression was noted in DMD cells, although this difference was primarily driven by a single pairwise comparison (DMD2 vs. CTL1; **Figure S6**) and was not consistent across all samples. By contrast, ANXA2 expression was significantly elevated in DMD myotubes, with an average increase of approximately 30% relative to

control (**Figure 4B; Figure S6**). These data confirm that ANXA2 is selectively upregulated in DMD muscle cells in vitro, while levels of ANXA1, ANXA5, and ANXA6 remain largely unchanged. Since ANXA2 interacts with dysferlin during membrane resealing [29], we investigated how excessive ANXA2 levels in skeletal muscle cells affect dysferlin expression. Consistent with previous reports [30], we observed that dysferlin expression is elevated in both DMD muscle biopsies and cell lines compared to controls **(Figure S7).** Similar to ANXA2, we hypothesize that myofibers upregulate dysferlin as a compensatory response to defective membrane repair mechanisms.

Given that mechanical stimulation enhances the membrane repair machinery in invasive cancer cells [18,31,32], we investigated the expression of annexins in myoblasts differentiated for 24 hours, either exposed or not to shear stress. We hypothesized that annexin overexpression in mechanically stressed muscle cells might reflect an adaptive response to anticipate sarcolemmal damage. DMD muscle cells were also included in the analysis; however, a significant experimental bias was acknowledged, as approximately 40% of DMD cells die upon exposure to shear stress **(see Figure S3).** As a result, potentially annexin-overexpressing cells may be lost during sample preparation and therefore excluded from the analysis. We quantified ANXA1, ANXA2, ANXA5, and ANXA6 expression in both control and DMD cell lines 24 hours after shear stress and compared these levels to those in unstressed cells **(Figure 5).** In control cells, shear stress led to a ~20% increase in ANXA5 and ANXA6 expression, while ANXA1 and ANXA2 levels remained unchanged **(Figure 5B).** These results suggest that mechanical stress selectively upregulates ANXA5 and ANXA6, potentially enhancing membrane repair capacity. As expected, DMD cells failed to upregulate ANXA5 and ANXA6 in response to shear stress, likely due to the loss of injured cells.

Together, our findings demonstrate that mechanical stress induces a significant increase in ANXA5 and ANXA6 expression in muscle cells derived from control individuals, suggesting that healthy muscle cells can enhance their membrane repair machinery in anticipation of future sarcolemmal injury. Furthermore, we showed dysregulated expression patterns of annexins in DMD cells. Notably, ANXA1 and ANXA2 are overexpressed in muscle biopsies from DMD patients. This upregulation was confirmed in cultured myotubes for ANXA2, and to a lesser extent for ANXA1.

3.3. Histological Distribution of Annexins is Disturbed in DMD Muscle

We next examined the localization of annexins in control and DMD muscle biopsies using immunohistofluorescence. In control samples, ANXA1 and ANXA2 were weakly and diffusely distributed within the cytoplasm of myofibers (**Figure 6 and Figure S9A-B**). Furthermore, ANXA2 was present in both the perimysium and the endothelium **(Figure 6 and Figure S9B).** In contrast, DMD biopsies showed increased extracellular localization of ANXA1 and, more markedly, ANXA2, suggesting

leakage from damaged myofibers (**Figure 6 and Figure S9A-B**). The absence of nuclear staining adjacent to ANXA1 and ANXA2 signals indicates that these annexins are unlikely to originate from infiltrating non-myogenic cells responding to muscle necrosis **(Figure 6, white arrows, and Figure S9A-B).** For ANXA5, we observed expression in only a subset of myofibers, where it was predominantly cytoplasmic (**Figure 6 and Figure S9C**). Co-immunostaining with fast myosin heavy chain revealed that ANXA5 expression was restricted to type II myofibers (**Figure S10A**). We found that the proportion of ANXA5-positive (or type II) myofibers was reduced to approximately 25% in DMD biopsies (**Figure S10B**). In control samples, ANXA6 was localized both in the cytoplasm and at the sarcolemma of muscle fibers (**Figure 6 and Figure S9D**). In DMD biopsies, ANXA6 was observed to accumulate at the sarcolemma in some myofibers, likely reflecting a response to membrane damage (**Figure 6**, white asterisks). Taken together, these findings indicate that DMD myofibers experience extensive sarcolemmal damage, associated with defective membrane repair mechanisms and the abnormal presence of annexins, particularly ANXA2, in the extracellular space. To further investigate whether ANXA2 is released from damaged and unrepaired DMD muscle cells, we analyzed the dynamics of GFP-tagged ANXA2 in laser-injured human skeletal muscle cells. In control cells, ANXA2 accumulates for several minutes within a broad sarcoplasmic region in close proximity to the disruption site after membrane injury (**Figure 7A–B**), consistent with its established role in lipid patch formation as previously described [20,29]. While ANXA2 also accumulated at the damage site in DMD cells (**Figure 7C–D**), the fluorescence intensity within the region surrounding this site was significantly lower than in control (**Figure 7E and Figure S11**). Because the overall intracellular trafficking of ANXA2 appeared comparable between injured control and DMD cells (**Figure S11**), the reduced signal at the damaged region in DMD myofibers likely reflects extracellular leakage of ANXA2, supporting the hypothesis of impaired membrane resealing.

3.4. Adipocyte Accumulation in DMD Biopsies

In LGMD2B, the presence of extracellular ANXA2 has been linked to enhanced muscle adipogenesis, partly through its influence onto FAPs [3]. To explore whether a similar process may contribute to disease progression in DMD, we analyzed the localization of perilipin, a lipid droplet-associated protein and marker of adipocytes, in skeletal muscle biopsies from control individuals and DMD patients. While perilipin staining was undetectable in control samples, DMD biopsies displayed extensive perilipin-positive areas, reflecting significant adipogenic infiltration (**Figure 8 and Figure S12**). These findings suggest that chronic membrane disruption and defective repair in DMD muscle fibers promote the release of cytosolic factors - such as ANXA2 or MMP-14[33] - into the extracellular space, which may in turn drive adipogenesis. This mechanism, previously described in LGMD2B [3], may thus be a common

feature of muscular dystrophies characterized by defective membrane repair, contributing to fatty degeneration of muscle tissue and functional decline.

4. Discussion

Here, we demonstrated that human DMD muscle cells are intrinsically defective in membrane repair, a critical function for maintaining muscle integrity during mechanical stress. Using a combination of histological, functional, and molecular analyses, we established that the sarcolemma fragility and the inability to effectively repair membrane lesions are key contributors to muscle cell death and progressive muscle loss in DMD. Through immunostaining of patient muscle biopsies, we confirmed that DMD muscle fibers frequently exhibit sarcolemmal injuries, as evidenced by the widespread intracellular presence of IgG, which was absent in control tissues. This observation is consistent with previous studies showing that dystrophin deficiency destabilizes the sarcolemma and severely compromises the mechanical stability of muscle fibers, making them highly susceptible to injury [9,34]. To specifically assess membrane repair capacity, we employed a recently developed muscle shear stress assay [19]. DMD muscle cells exhibited a significantly higher proportion of damaged and unrepaired cells compared to controls, reaching levels similar to those seen in LGMD2B, a known membrane repair-deficient disease [2]. Crucially, the shear stress experiments in Ca^{2+}-free conditions showed no difference in intrinsic membrane fragility between DMD and control cells, indicating that the defect lies in the repair process itself rather than in increased mechanical vulnerability. However, this conclusion applies only within this experimental context, which is far from physiological conditions. In vivo, DMD patient muscle fibers may experience both increased fragility and defective membrane repair. Finally, we corroborated the impaired membrane repair capacity of DMD muscle cells through laser irradiation experiments on differentiated myotubes. Jaiswal and collaborators previously emphasized the role of mitochondria in membrane repair and identified mitochondrial dysfunction as a key contributor to DMD pathology in the mdx mouse model [12]. In dystrophin-deficient murine muscle fibers, mitochondrial dynamics and function were compromised, leading to ineffective repair and increased myofiber death. A comparable mechanism is likely at play in human DMD. Together, these findings firmly establish that, similar to LGMD2B, the fundamental defect in human DMD resides in defective membrane repair of skeletal muscle cells.

At the molecular level, we found that annexin expression is dysregulated in DMD muscle. In biopsies, ANXA1 and ANXA2 were significantly overexpressed, while ANXA5 and ANXA6 showed only modest changes. This aligns with previous findings in both human DMD samples [4] and mdx mice [12]. Under cell culture conditions, only ANXA2 was consistently overexpressed in DMD myotubes, while ANXA1 levels

remained similar between DMD and control cells. Since annexin overexpression alone is insufficient to restore membrane repair capacity in DMD muscle cells, we conclude that a key component of the membrane repair machinery—likely playing a distinct role from ANXA1 and ANXA2—is still missing and remains to be identified. Immunofluorescence analyses further revealed that the subcellular distribution of annexins is disrupted in DMD muscle. While ANXA1 and ANXA2 were diffusely cytoplasmic in controls, they were observed in the extracellular milieu in DMD samples, suggesting that membrane lesions allow annexin leakage. Interestingly, ANXA2 was particularly abundant outside myofibers in DMD tissue. Consequently, defects in membrane repair not only lead to direct myofiber degeneration but also initiate secondary pathological cascades involving the muscle environment. In this regard, it has been reported that in LGMD2B, persistent membrane damage promotes the activation and pathological differentiation of FAPs, contributing significantly to fatty infiltration and muscle loss [3]. A similar mechanism may occur in DMD, where defective membrane repair could lead to abnormal activation of FAPs, promoting adipocyte accumulation and worsening muscle degeneration. A previous work has indeed reported a significant expansion of the FAP population in muscle biopsies from DMD patients compared to healthy controls [35]. To further investigate this hypothesis, we performed perilipin immunohistofluorescence on control and DMD patient biopsies and found that DMD is associated with accumulation of adipocytes in the muscle interstitium. Collectively, our results establish that human DMD muscle cells have a true intrinsic defect in membrane repair. This defect is associated with abnormal annexin expression and distribution, particularly of ANXA2, and contributes to the progressive loss of muscle fibers observed in patients. Our findings highlight ANXA2 as a potential therapeutic target in DMD. Strategies that aimed at selectively inhibiting extracellular ANXA2 could offer new avenues to slow disease progression by preventing adipogenesis.

Authors Contributions

M.L.Q. performed the majority of experiments on muscle biopsies with assistance from J.R. and C.G (western-blot analysis) and S.D. (immunohistochemistry). L.A performed the majority of experiments on muscle cell lines with assistance from P.R. (western-blot analysis and shear stress assays), F.B. and A.S. (cell culture and western-blot analysis). R.C. performed western-blot analysis of dysferlin and dystrophin and membrane repair assays by laser ablation. K.M. established the AB1098 and 6594 cell lines. F.L. and N.B. conducted western blot analyses to identify DMD cases and quantify dysferlin expression. G.S. and M.L.M.N. were responsible for the establishment and long-term management of the biobank providing human muscle biopsies. A.B. coordinated the entire project and designed the experiments. A.B. wrote the manuscript with the help of M.L.M.N. and M.L.Q.

Funding

This research was funded by AFM-telethon (grant 22442 to A.B., grant 24991 to A.B. and M.L.M.N. and grant 23881 to L.A.).

Acknowledgments

The authors acknowledge the AFM-telethon association for its financial support (Grant 23881 to L.A. and 22442 and 24991 to A.B. and M-L.M-N). The authors thank the Centre de Ressources Biologiques Plurithematique of the Bordeaux University Hospital (BB-0033-00094) for providing the material used in this research. We are also deeply grateful to the COLMYONEU muscle bank donors for their generous donation of the tissue samples used in this study. The HistoCARE facility of IMN (UMR5293, unit of the CNRS and Bordeaux University) is acknowledged for performing part of the IHC experiments. The authors wish to acknowledge MyoLine, the platform for the immortalization of human cells from the Institute of Myology in Paris for the establishment of muscle cell lines. Christel Poujol and Sébastien Marais are acknowledged for the help in studies of trafficking of ANXA2 and membrane repair assay by laser ablation that were done in the Bordeaux Imaging Center a service unit of the CNRS-INSERM and Bordeaux University, member of the national infrastructure France BioImaging supported by the French National Research Agency (ANR-10-INBS-04).

Ethic statement

This study has been approved by the appropriate ethics committee and has therefore been performed in accordance with the ethical standards laid down in the 1964 Declaration of Helsinki and its later amendments. All patients gave their informed consent prior to their inclusion in the study.

Conflicts of interest

The authors declare no conflicts of interest.

Bibliography

1. McNeil PL, Steinhardt RA. Plasma membrane disruption: repair, prevention, adaptation. *Annu Rev Cell Dev Biol* 2003;**19**:697–731.
2. Bansal D, Miyake K, Vogel SS, Groh S, Chen C-C, Williamson R *et al.* Defective membrane repair in dysferlin-deficient muscular dystrophy. *Nature* 2003;**423**:168–172.
3. Hogarth MW, Defour A, Lazarski C, Gallardo E, Manera JD, Partridge TA *et al.* Fibroadipogenic progenitors are responsible for muscle loss in limb girdle muscular dystrophy 2B. *Nat Commun* 2019;**10**.

4. Cagliani R, Magri F, Toscano A, Merlini L, Fortunato F, Lamperti C *et al.* Mutation finding in patients with dysferlin deficiency and role of the dysferlin interacting proteins annexin A1 and A2 in muscular dystrophies. *Hum Mutat* 2005;**26**:283.

5. Novak ML, Weinheimer-Haus EM, Koh TJ. Macrophage activation and skeletal muscle healing following traumatic injury. *Journal of Pathology* 2014;**232**:344–355.

6. Joe AWB, Yi L, Natarajan A, Le Grand F, So L, Wang J *et al.* Muscle injury activates resident fibro/adipogenic progenitors that facilitate myogenesis. *Nature Cell Biology 2010 12:2* 2010;**12**:153–163.

7. Hoffman EP, Brown RH, Kunkel LM. Dystrophin: the protein product of the Duchenne muscular dystrophy locus. *Cell* 1987;**51**:919–928.

8. Ervasti JM, Campbell KP. Membrane organization of the dystrophin-glycoprotein complex. *Cell* 1991;**66**:1121–1131.

9. Petrof BJ, Shrager JB, Stedman HH, Kelly AM, Sweeney HL. Dystrophin protects the sarcolemma from stresses developed during muscle contraction. *Proc Natl Acad Sci U S A* 1993;**90**:3710–3714.

10. Wallace GQ, McNally EM. Mechanisms of muscle degeneration, regeneration, and repair in the muscular dystrophies. *Annu Rev Physiol* 2009;**71**:37–57.

11. Jungbluth H, Treves S, Zorzato F, Sarkozy A, Ochala J, Sewry C *et al.* Congenital myopathies: disorders of excitation-contraction coupling and muscle contraction. *Nat Rev Neurol* 2018;**14**:151–167.

12. Vila MC, Rayavarapu S, Hogarth MW, Van der Meulen JH, Horn A, Defour A *et al.* Mitochondria mediate cell membrane repair and contribute to Duchenne muscular dystrophy. *Cell Death Differ* 2017;**24**:330–342.

13. Collins CA, Morgan JE. Duchenne's muscular dystrophy: animal models used to investigate pathogenesis and develop therapeutic strategies. *Int J Exp Pathol* 2003;**84**:165–172.

14. Mamchaoui K, Trollet C, Bigot A, Negroni E, Chaouch S, Wolff A *et al.* Immortalized pathological human myoblasts: towards a universal tool for the study of neuromuscular disorders. *Skelet Muscle* 2011;**1**:34.

15. Echigoya Y, Lim KRQ, Melo D, Bao B, Trieu N, Mizobe Y *et al.* Exons 45-55 Skipping Using Mutation-Tailored Cocktails of Antisense Morpholinos in the DMD Gene. *Mol Ther* 2019;**27**:2005–2017.

16. Tasca F, Brescia M, Liu J, Janssen JM, Mamchaoui K, Gonçalves MAFV. High-capacity adenovector delivery of forced CRISPR-Cas9 heterodimers fosters precise chromosomal deletions in human cells. *Mol Ther Nucleic Acids* 2023;**31**:746–762.

17. Carmeille R, Bouvet F, Tan S, Croissant C, Gounou C, Mamchaoui K *et al.* Membrane repair of human skeletal muscle cells requires Annexin-A5. *Biochim Biophys Acta Mol Cell Res* 2016;**1863**:2267–2279.

18. Bouvet F, Ros M, Bonedeau E, Croissant C, Frelin L, Saltel F *et al.* Defective membrane repair machinery impairs survival of invasive cancer cells. *Sci Rep* 2020;**10**:21821.

19. d'Agata L, Rassinoux P, Gounou C, Bouvet F, Bouragba D, Mamchaoui K *et al.* A Novel Assay Reveals the Early Setting-Up of Membrane Repair Machinery in Human Skeletal Muscle Cells. *J Cell Biochem* 2024;**126**:e30.

20. Croissant C, Gounou C, Bouvet F, Tan S, Bouter A. Trafficking of Annexins during Membrane Repair in Human Skeletal Muscle Cells. *Membranes 2022, Vol 12, Page 153* 2022;**12**:153.

21. Bencze M, Periou B, Baba-Amer Y, Authier FJ. Immunolabelling Myofiber Degeneration in Muscle Biopsies. *J Vis Exp* 2019;**2019**.

22. Heydemann A, Huber JM, Demonbreun A, Hadhazy M, McNally EM. Genetic background influences muscular dystrophy. *Neuromuscular Disorders* 2005;**15**:601–609.

23. Quattrocelli M, Capote J, Ohiri JC, Warner JL, Vo AH, Earley JU *et al.* Genetic modifiers of muscular dystrophy act on sarcolemmal resealing and recovery from injury. *PLoS Genet* 2017;**13**:e1007070.

24. Vilchez JJ, Gallano P, Gallardo E, Lasa A, Rojas-García R, Freixas A *et al.* Identification of a novel founder mutation in the DYSF gene causing clinical variability in the spanish population. *Arch Neurol* 2005;**62**:1256–1259.

25. Swaggart KA, Demonbreun AR, Vo AH, Swanson KE, Kim EY, Fahrenbach JP *et al.* Annexin A6 modifies muscular dystrophy by mediating sarcolemmal repair. *Proc Natl Acad Sci U S A* 2014;**111**:6004–6009.

26. Demonbreun AR, Allen M V, Warner JL, Barefield DY, Krishnan S, Swanson KE *et al.* Enhanced Muscular Dystrophy from Loss of Dysferlin Is Accompanied by Impaired Annexin A6 Translocation after Sarcolemmal Disruption. 2016;**186**:1610–1622.

27. Babiychuk EB, Monastyrskaya K, Burkhard FC, Wray S, Draeger A. Modulating signaling events in smooth muscle: cleavage of annexin 2 abolishes its binding to lipid rafts. *The FASEB Journal* 2002;**16**:1177–1184.

28. Wang CY, Lin CF. Annexin A2: Its molecular regulation and cellular expression in cancer development. *Dis Markers* 2014;**2014**.

29. Lennon NJ, Kho A, Bacskai BJ, Perlmutter SL, Hyman BT, Brown RH. Dysferlin interacts with annexins A1 and A2 and mediates sarcolemmal wound-healing. *J Biol Chem* 2003;**278**:50466–50473.

30. Vontzalidis A, Terzis G, Manta P. Increased dysferlin expression in Duchenne muscular dystrophy. *Anal Quant Cytopathol Histpathol* 2014;**36**:15–22.

31. Gounou C, Bouvet F, Liet B, Prouzet-Mauléon V, D'Agata L, Harté E *et al.* Annexin-A5 and annexin-A6 silencing prevents metastasis of breast cancer cells in zebrafish. *Biol Cell* 2023;**115**:e202200110.

32. Gounou C, Rouyer L, Siegfried G, Harté E, Bouvet F, d'Agata L *et al.* Inhibition of the membrane repair protein annexin-A2 prevents tumor invasion and metastasis. *Cellular and Molecular Life Sciences* 2024;**81**:1–16.

33. Kopinke D, Roberson EC, Reiter JF. Ciliary Hedgehog Signaling Restricts Injury-Induced Adipogenesis. *Cell* 2017;**170**:340-351.e12.

34. Carmignac V, Durbeej M. Cell-matrix interactions in muscle disease. *J Pathol* 2012;**226**:200–218.

35. Cardone N, Taglietti V, Baratto S, Kefi K, Periou B, Gitiaux C *et al.* Myopathologic trajectory in Duchenne muscular dystrophy (DMD) reveals lack of regeneration due to senescence in satellite cells. *Acta Neuropathol Commun* 2023;**11**.

Figures

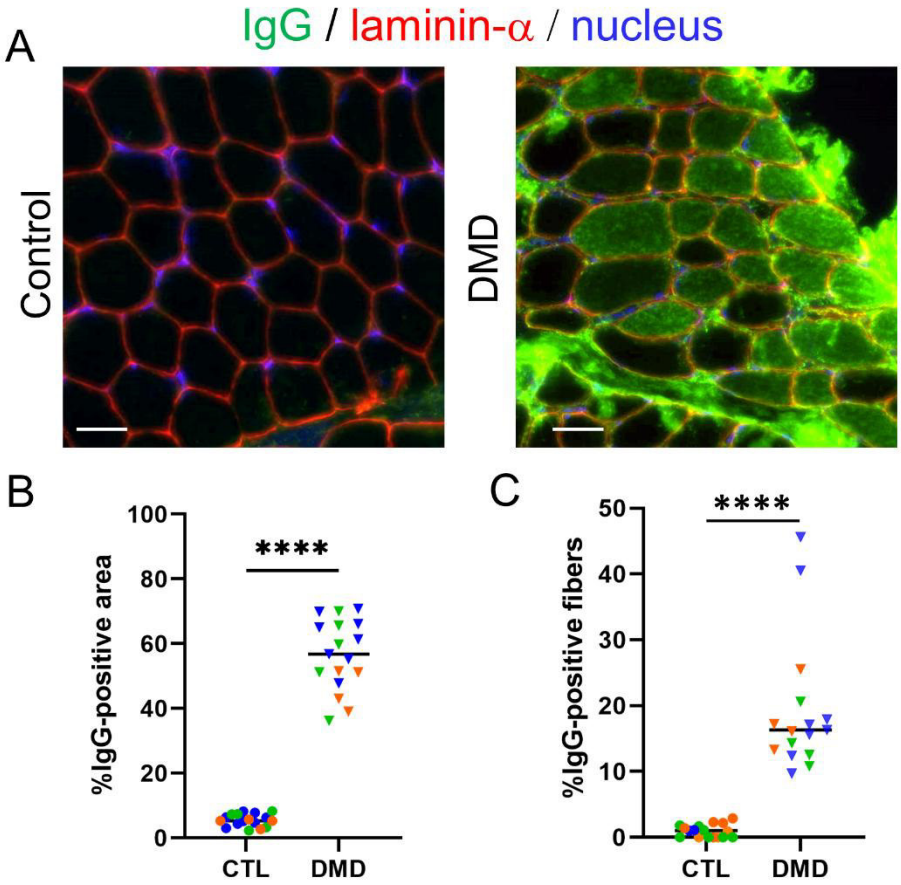

FIGURE 1 Impaired sarcolemma integrity in patients with DMD. A) Sarcolemma integrity was assessed by IgG staining (green) in skeletal muscle samples from control and DMD patients. Co-staining of laminin (red, basal lamina) and Hoechst (blue, nucleus) was also performed. Scale bar = 20 µm. B-C) The percentage of area with IgG positivity (B) and IgG-positive fibers (C) was calculated for control (circles, n=3) and DMD patients (inverted triangles, n=3). Each color corresponds to a control individual or a patient. Mann-Whitney test. ****$p < 0.0001$.

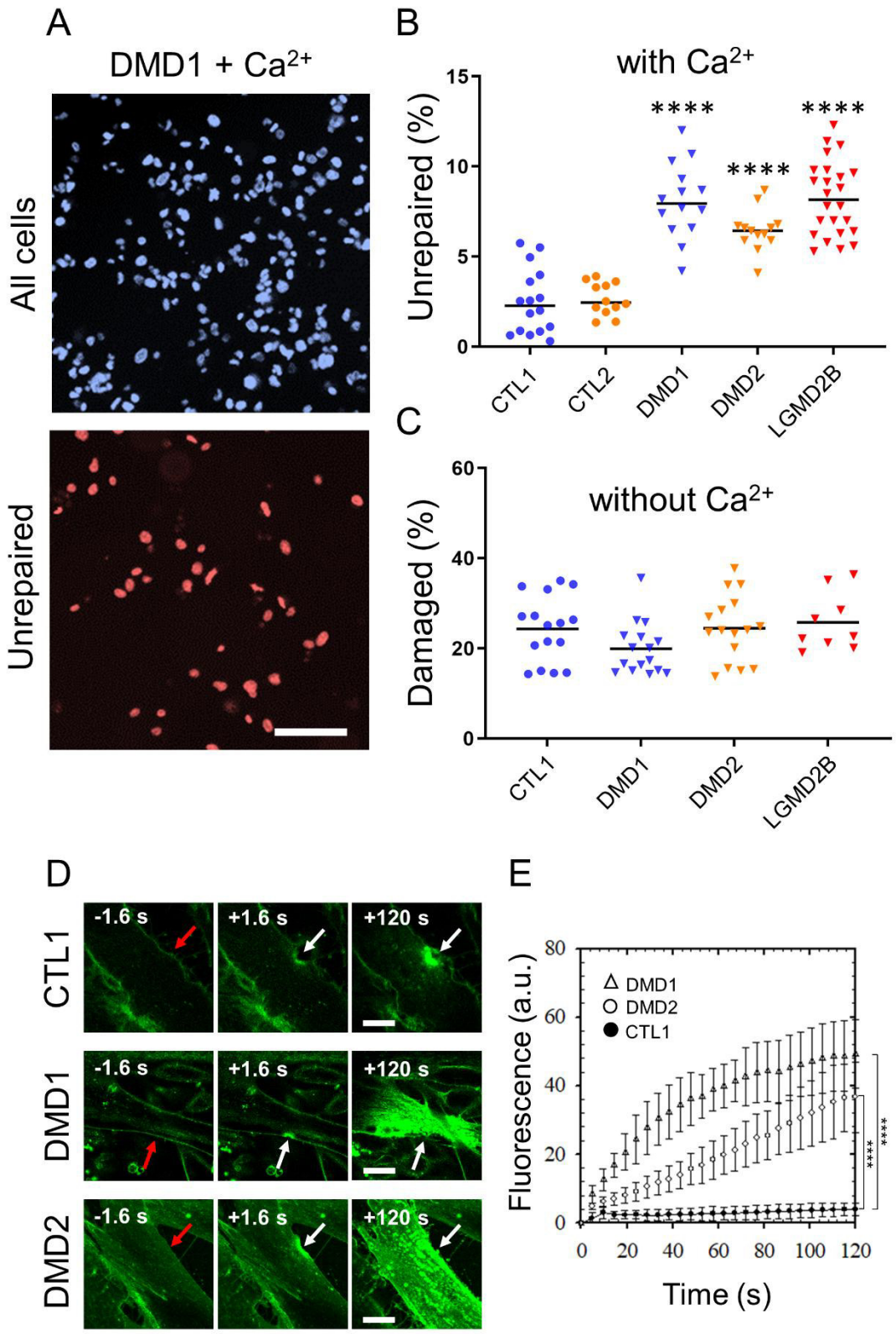

FIGURE 2 Identification of defective membrane repair process in human DMD muscle cells. A) Control, DMD and LGMD2B cell lines were subjected to the muscle shear stress assay and propidium iodide (PI, red) permeability assay was performed to quantify unrepaired cells. Hoechst was used to stain all the cells (blue). Example of images acquired for DMD1 cells submitted to the shear stress muscle assay in

the presence of Ca^{2+}. B-C) Scatter plots with the mean value representing PI-positive cells when the shear stress assay was performed in the presence of 2mM Ca^{2+} (B) or the absence of free Ca^{2+} (C) for control (circles, n = 16), DMD (inverted triangle, n = 16), and LGMD2B (red inverted triangle, n = 24 in B and n = 9 in C). Mann-Whitney test using CTL1 cells as a reference. **** $p < 0.0001$. D) Sequences of representative images showing the response of control (CTL) or DMD myotubes to a membrane damage performed by 110-mW infrared laser irradiation, in the presence of FM1-43 (green). In all figures, the area of membrane irradiation is marked with a red arrow before irradiation and a white arrow after irradiation. Scale bars: 10 µm. E) Kinetic data represent the FM1−43 fluorescence intensity for control (black filled circles) or DMD1 (empty triangles) or DMD2 (empty circles) myotubes, integrated over whole cell sections, averaged for about 20 cells analyzed in three independent experiments (+/−SEM). Kolmogorov-Smirnov test performed either between CTL1 and DMD1 or CTL1 and DMD2. ****: $p < 0.0001$.

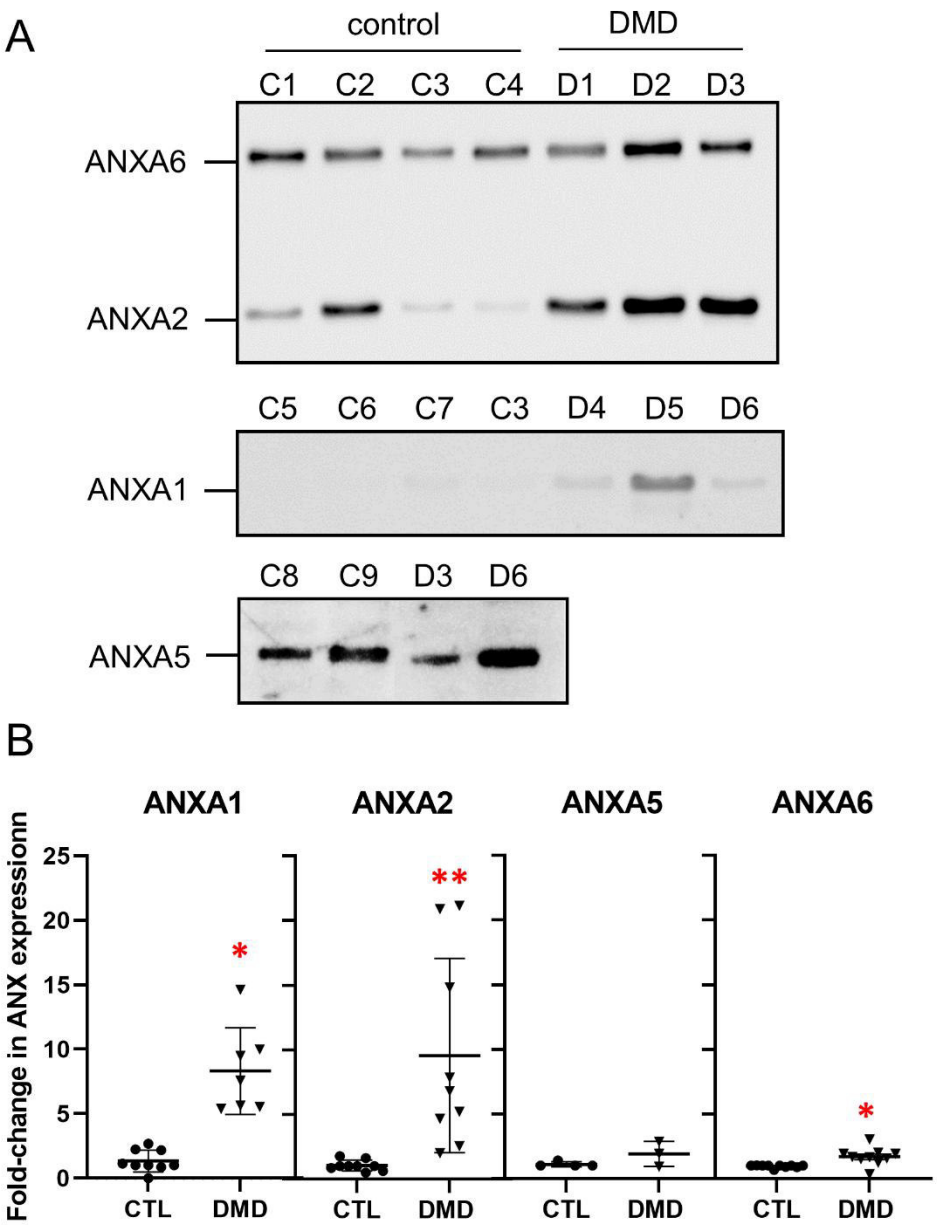

FIGURE 3 Annexin expression in control and DMD skeletal muscle biopsies. A) Annexin expression was quantified by western-blot analysis. Normalization was performed by total protein detection (see Figure S4A). Full membranes are presented in supplementary Figure S4A. B) Annexin expression quantified by western-blot analysis from biopsies of control individuals or DMD patients. Data were normalized to total protein, using a control biopsy as the internal control. Each circle or triangle represents an individual or patient, respectively. Figure S4B shows the ANXA5 and ANXA6 plots with the vertical axis scale adjusted to better highlight the differences. Wilcoxon signed rank test. *: $p < 0.05$; **: $p < 0.01$.

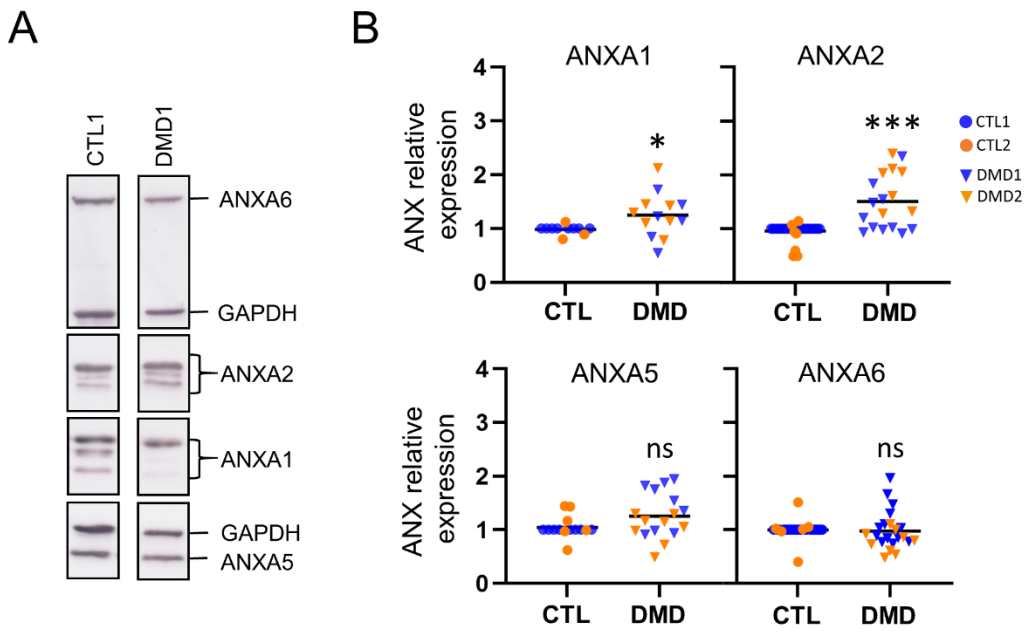

FIGURE 4 Annexin expression in control and DMD skeletal muscle cell lines. A) Annexin expression was quantified by western-blot analysis from myotubes. Each sample was systematically analyzed on four independent membranes for detecting ANXA1, ANXA2, ANXA5 or ANXA6. As ANXA1 and ANXA2 molecular weight is similar to GAPDH, this loading control was immunodetected only on ANXA5 and ANXA6 membranes. The full membranes are presented in supplementary Figure S5. B) Data were systematically normalized with GAPDH and CTL1 was used as an internal control. Wilcoxon signed rank test using CTL1 as a reference. *: $p < 0.05$; ***: $p < 0.001$.

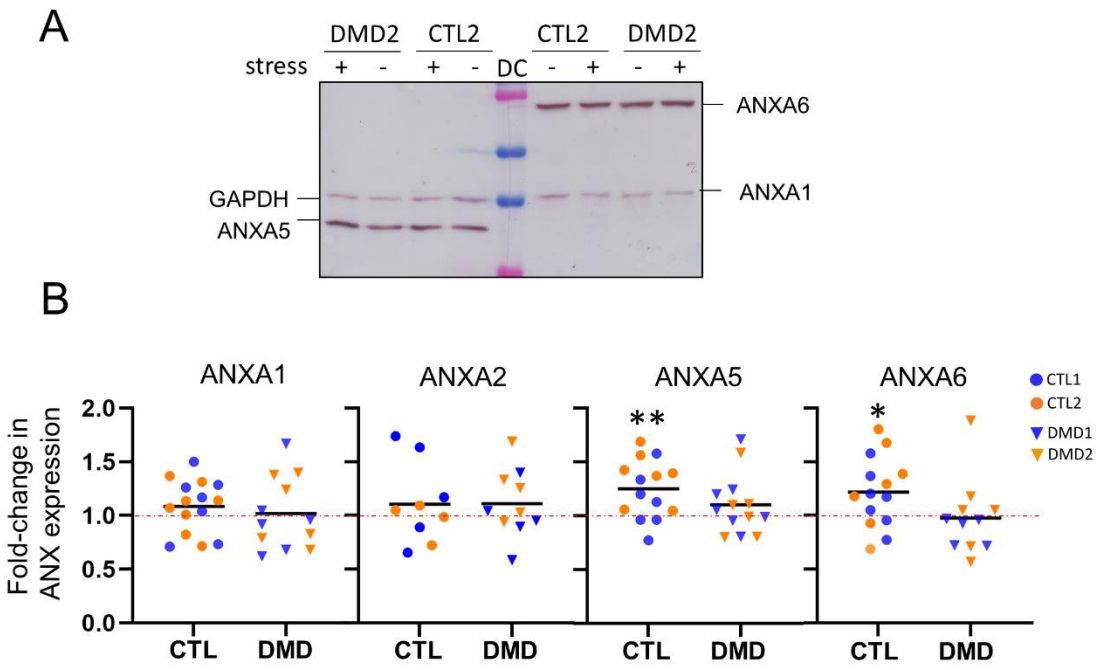

FIGURE 5 Annexin expression in control and DMD skeletal muscle cells submitted to shear stress. A) Example of western blot analyzing the expression of ANXA1, ANXA5, and ANXA6 in CTL2 and DMD2 cell lines submitted (+) or not (-) to shear stress. GAPDH has been detected as a loading control. The Dual color molecular weight marker (DC) has been used. B) Scatter plot with mean value displaying the fold-change of annexin expression in control and DMD skeletal muscle cell lines after shear stress normalized for the basal unstressed condition. The dashed red line indicates the baseline corresponding to the absence of annexin expression after shear stress. Data obtained on each cell line are presented in Figure S8. Wilcoxon test. *: $p < 0.05$; **: $p < 0.01$.

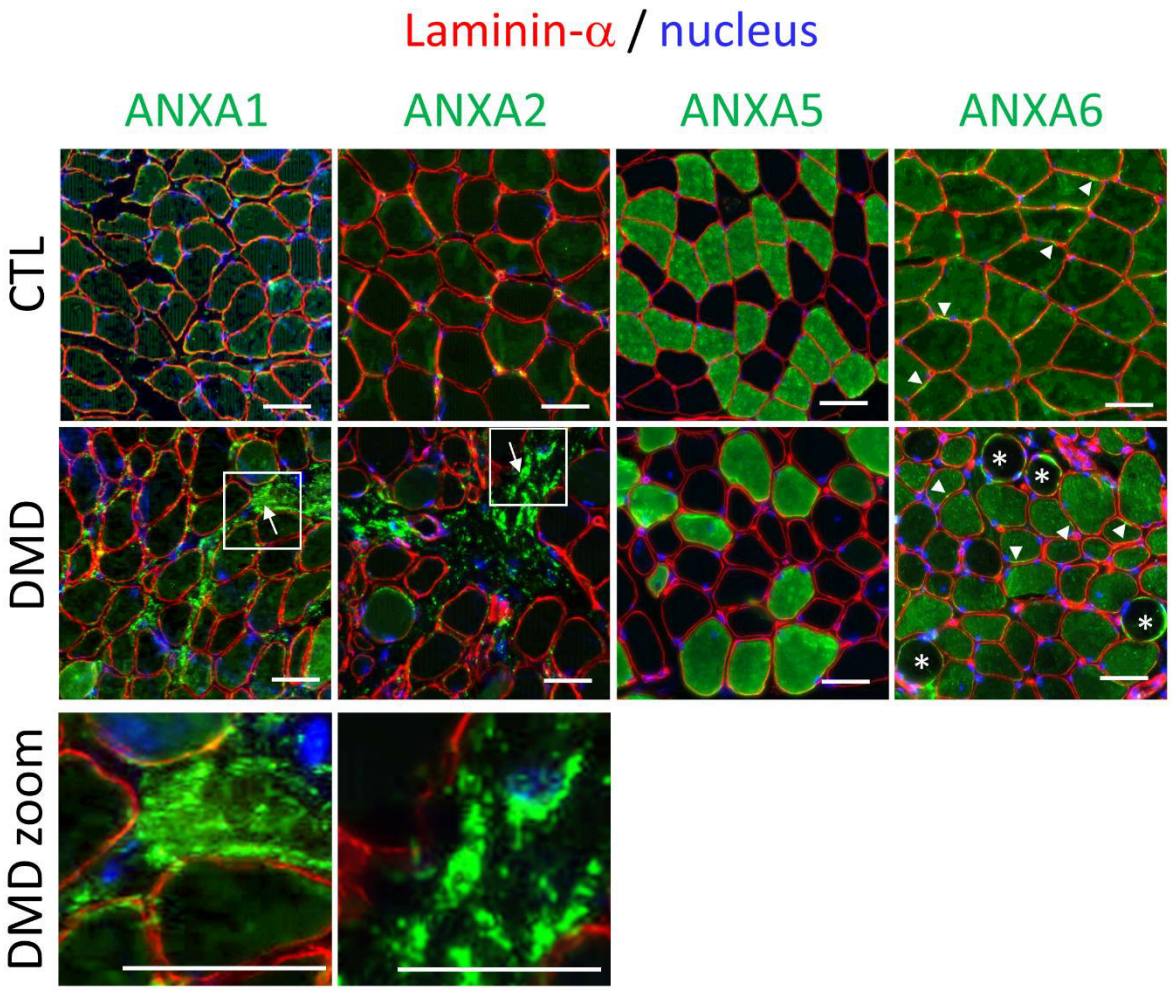

FIGURE 6 Analysis of annexin distribution in control and DMD biopsies. Distribution of annexin in control (n=3) and DMD (n=3) biopsies was analyzed by immunohistofluorescence. Laminin-α (red) was immunostained to detect sarcolemma. Cell nuclei were stained with Hoechst 33342 (blue). White arrows indicate extracellular areas devoid of non-myogenic cells with ANXA1 or ANXA2 staining. The magnified views (DMD zoom) correspond to the area enclosed by the white squares. Arrowheads indicate discrete regions of the sarcolemma exhibiting ANXA6 colocalization. White asterisks indicate myofibers where ANXA6 concentrated at the sarcolemma. Scale bar = 50 µm.

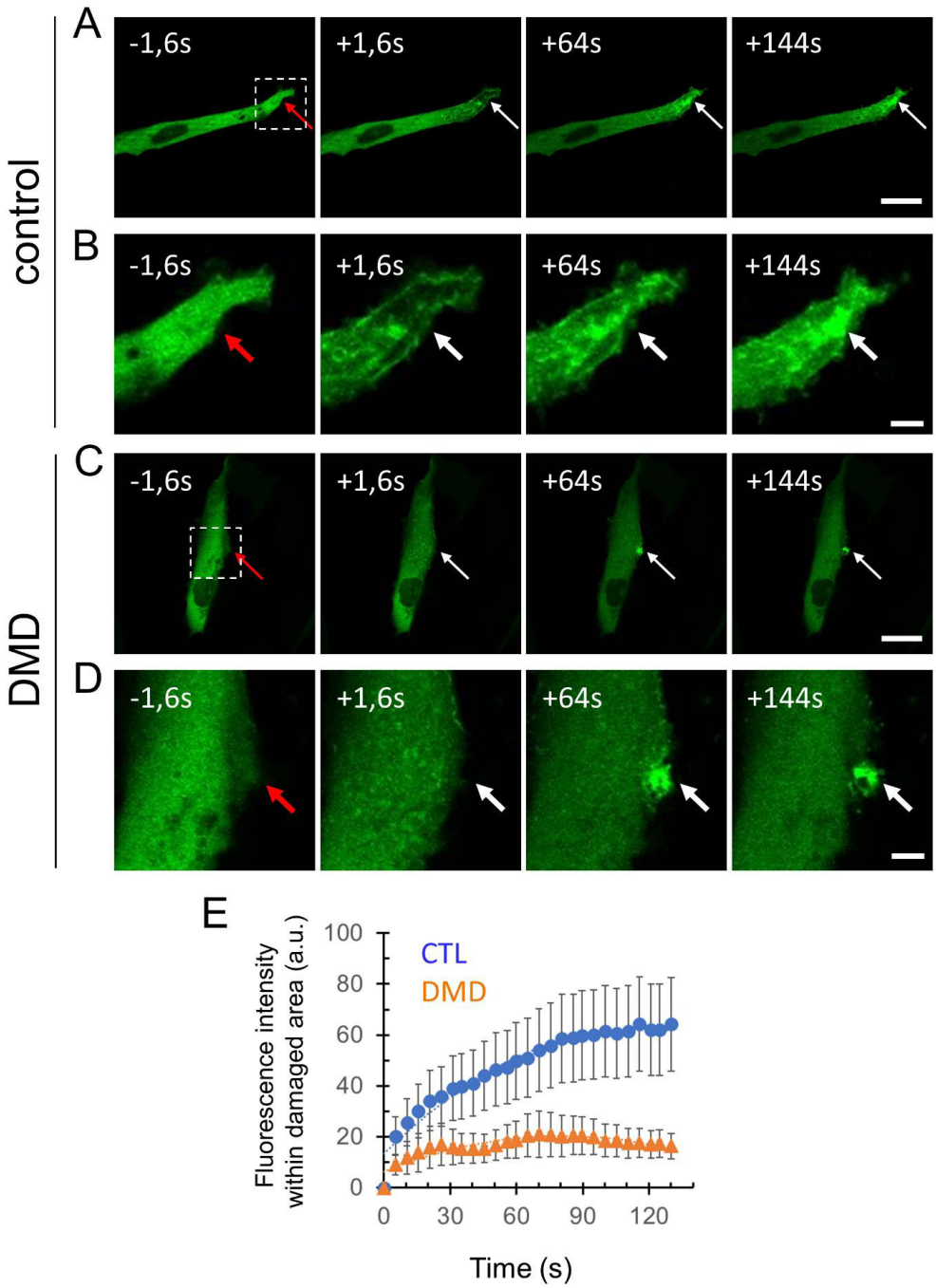

FIGURE 7 Trafficking of ANXA2 in control or DMD skeletal muscle cells damaged by laser ablation. A-B) ANXA2-GFP expressing CTL1 24-hour-differentiated myoblasts were damaged by laser ablation. In B, magnified images of the area framed (dotted line) in A. C-D) ANXA2-GFP expressing DMD1 24-hour-differentiated myoblasts were damaged by laser ablation. In D, magnified images of the area framed (dotted line) in C. Red arrow, area before irradiation; white arrow, area after irradiation. Scale bar for images A and C: 15 µm, B and D: 2.5 µm. E) Traffic of ANXA2-GFP at the disruption site. Data (mean ± SD) represent the ANXA2-GFP fluorescence intensity integrated over a 10 µm-diameter ROI (see Figure S11A), which is plotted versus time. Circular ROI was drawn from the damaged site toward the cytoplasm. For CTL and DMD 24-hour-differentiated myoblasts, n = 6.

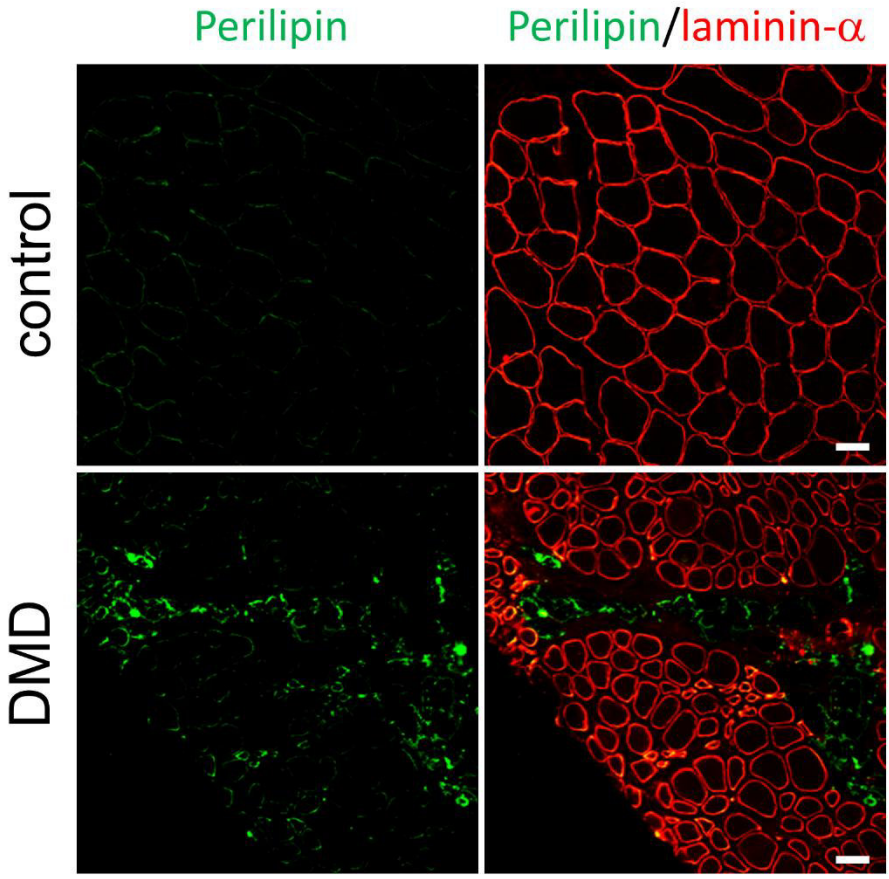

FIGURE 8 Analysis of perilipin distribution in control and DMD biopsies. Distribution of perilipin (green) in control (n=3) and DMD (n=3) biopsies was analyzed by immunohistofluorescence. Laminin−α (red) was also immunostained to detect sarcolemma. Scale bar = 50 µm.

SUPPLEMENTARY MATERIAL FOR:

Duchenne muscular dystrophy is driven by defective membrane repair and annexin-A2 dysregulation in skeletal muscle

Mégane Le Quang[1,2,8*], Léna d'Agata[1*], Romain Carmeille[1], Phoebe Rassinoux[1,3], Joana Ruiz[1], Céline Gounou[1], Antoine Salesses[1], Flora Bouvet[1], Kamel Mamchaoui[4], Sandra Dovero[5], Nathalie Deburgrave[6], France Leturcq[6], Guilhem Solé[7], Marie-Laure Martin-Négrier[2,7,8] and Anthony Bouter[1**]

[1]Univ. Bordeaux, CNRS, Bordeaux INP, CBMN, UMR 5248, F-33600 Pessac, France.

[2]Department of Pathology, University Hospital (CHU) of Bordeaux, Pellegrin Hospital, Place Amélie Raba Léon, 33000, Bordeaux, France.

[3]present address: Institut NeuroMyogène (INMG) - Laboratoire Physiopathologie et Génétique du Neurone et du Muscle, Université Claude Bernard Lyon 1, CNRS UMR 5261, INSERM U1315, Lyon, France.

[4]Sorbonne Université, Inserm, Institut de Myologie, Centre de Recherche en Myologie, F-75013, Paris, France.

[5]Univ. Bordeaux, CNRS, HistoCARE Facility, IMN, UMR 5293, Bordeaux, France.

[6]Service de Medecine Genomique, Maladies de Systeme et d'Organe-Federation de Genetique et de Medecine Genomique, DMU BioPhyGen, APHP Centre-Universite Paris Cite-Hopital Cochin, Paris, France.

[7]Centre de Référence des Maladies Neuromusculaires AOC, Service de Neurologie et Maladies Neuromusculaires, FILNEMUS, EURONMD, Hôpital Pellegrin, CHU de Bordeaux, France.

[8]Univ. Bordeaux, CNRS, IMN, UMR 5293, Bordeaux, France.

*Contribute equally to this work

**Corresponding author, e-mail: anthony.bouter@u-bordeaux.fr; phone: +33 540006860

Running title: Membrane repair and annexins in DMD

Case	Age (years)	Sex	Biopsy site	Age at symptom onset	CPK at diagnosis (IU/L)	Biopsy year	Genetic findings (in the *DMD* gene)
1	4	M	Quadriceps	<1 year	22634	2021	Nonsense variant in exon 52 resulting in a premature stop codon
2	6	M	Quadriceps	1 year	24556	2020	Out-of-frame deletion encompassing exons 45–50
3	4	M	Quadriceps	1 year	22267	2020	Tandem duplication of exons 6 and 7
4	6	M	Deltoid	<1 year	16546	2020	Splice-site variant affecting exon 66
5	5	M	Quadriceps	Not reported	16633	2019	Nonsense mutation in exon 43
6	9	M	Deltoid	3 years	8145	2019	Hemizygous duplication of exon 2
7	9	M	Deltoid	4 years	13251	2018	Single-nucleotide deletion within exon 13
8	8	M	Deltoid	4 years	17534	2018	Indel (insertion-deletion) mutation in exon 56
9	4	M	Quadriceps	<1 year	22889	2015	Out-of-frame deletion spanning exons 45–52
10	4	M	Quadriceps	<1 year	21979	2015	Frameshift-causing deletion of exons 8 through 11

Table S1. Clinical data of DMD cases. CPK: Creatine phosphokinase. M: Male

Case	Dystrophin (central domain)*	Dystrophin (C-terminal domain)*	Dysferlin*,[1]	γ-Sarcoglycan*	α-Sarcoglycan*	Calpain-3 (94 kDa)*	Calpain-3 (30 kDa)*	Calpain-3 (60 kDa)*
1	Absent	Absent	Present	Severely reduced	Severely reduced	Present	Present	Present
2	NA**	NA**	NA**	NA**	NA**	NA**	NA**	NA**
3	Absent	Absent	Present	Reduced	Reduced	Present	Present	Present
4	Absent	Absent	Present	Reduced	Reduced	Reduced	Reduced	Present
5	Absent	Absent	Present	Reduced	Reduced	Present	Present	Present
6	Absent	Absent	Present	Reduced	Reduced	Present	Present	Present
7	Absent	Absent	Present	Reduced	Reduced	Reduced	Present	Present
8	Absent	Absent	Present	Reduced	Reduced	Present	Present	Present
9	Absent	Absent	Present	Reduced	Reduced	Present	Present	Present
10	Absent	Absent	Present	Reduced	Reduced	Present	Present	Present

Table S2. Western Blot analysis of DMD cases. *Western blot-based protein analysis performed on human muscle biopsy specimens. **Not assessed – direct genetic testing following biopsy. [1]Western Blot quantification of dysferlin is presented in Figure S7.

Case	Age (years)	Sex	Biopsy site
1	35	F	deltoïde
2	7	M	deltoïde
3	25	M	deltoïde
4	43	M	quadriceps
5	4	M	quadriceps
6	50	F	deltoïde
7	16	F	quadriceps
8	2	M	quadriceps
9	68	F	quadriceps
10	6	M	quadriceps

Table S3. Clinical data of control cases. M: Male; F: Female.

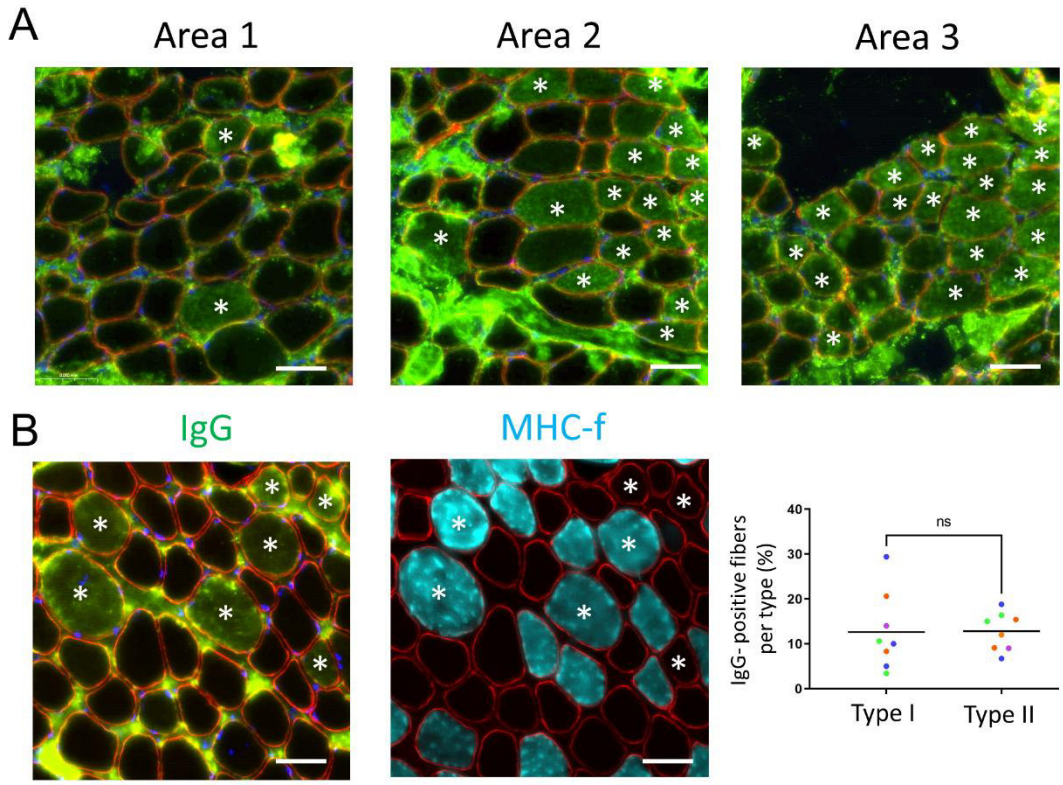

FIGURE S1 IgG staining in DMD muscle biopsy. A) Three different areas of a DMD muscle biopsy immunostained for IgG (Green) were presented to assess staining heterogeneity. B) Representative co-immunostaining for intracellular IgG (green) and fast myosin heavy chain (MHC-f, blue) to distinguish type II (MHC-f^{+}) and type I (MHC-f^{-}) myofibers. The proportion of IgG-positive myofibers among type I and type II fibers is shown in scatter plots with mean values. Data represent two areas from each of four independent DMD muscle biopsies; each color indicates one biopsy. Mann-Whitney test. Laminin-α (red) was also immunostained to detect sarcolemma. White asterisks mark IgG-positive fibers. Scale bars = 40 µm.

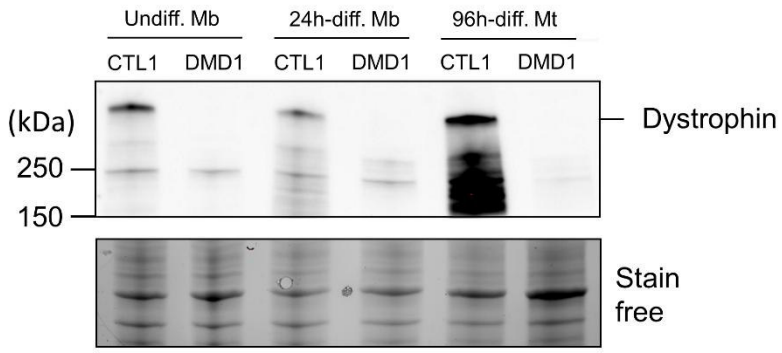

FIGURE S2 Dystrophin expression in control and DMD skeletal muscle cell lines. Dystrophin expression was quantified by western-blot analysis (upper image). 20 µg protein extracts were separated on SDS-PAGE using 4–15% Mini-PROTEAN® TGX™ precast protein gels (Biorad) and the Precision Plus Protein All Blue Standards (Bio-Rad). Electrophoretic transfer onto PVDF membrane was performed with the Trans-Blot Turbo Transfer System (BioRad) during 15 min at 1.3A/25V. Total protein signals (lower image) were measured using the Chemi-Doc imager (Bio-Rad) and ImageLab software. Revelation was performed by chemiluminescence using secondary antibodies conjugated to horse-radish peroxidase (GE-Healthcare) diluted 1:2000 in saturation solution and Clarity™ Western ECL substrate (Bio-Rad). Analysis was performed on undifferentiated myoblasts (Undiff. Mb), 24h-diferentiated myoblasts (24h-diff. Mb), and 96h-differentiated myotubes (96h-diff. Mt). As previously reported, dystrophin is expressed not only in differentiated myotubes but also in myoblasts, particularly in myoblast cell lines derived from satellite cells (Dumont et al. 2015 Nat Med. 21(12):1455–1463; Franzmeier et al. 2025 Cells 14(12), 892).

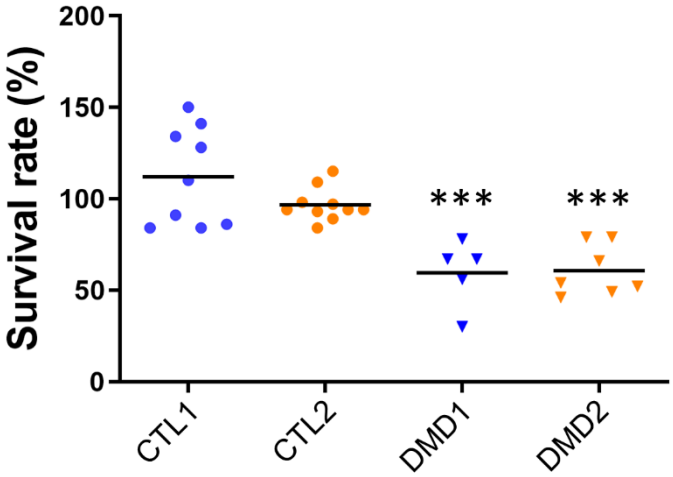

FIGURE S3 Reduced survival rate of DMD cells after membrane damage. For each experiment, cells were divided into two populations: one underwent shear stress, while the other remained in resting condition. After the shear stress treatment, cells were seeded in growth condition for 24h. Necrotic cells were then quantified by Trypan blue staining and Thoma hematimeter. The survival rate corresponds to the ratio of the number of living cells between the population subject to shear stress and the resting population. Mann-Whitney test using CTL1 cells as a reference. ***: $p < 0.001$.

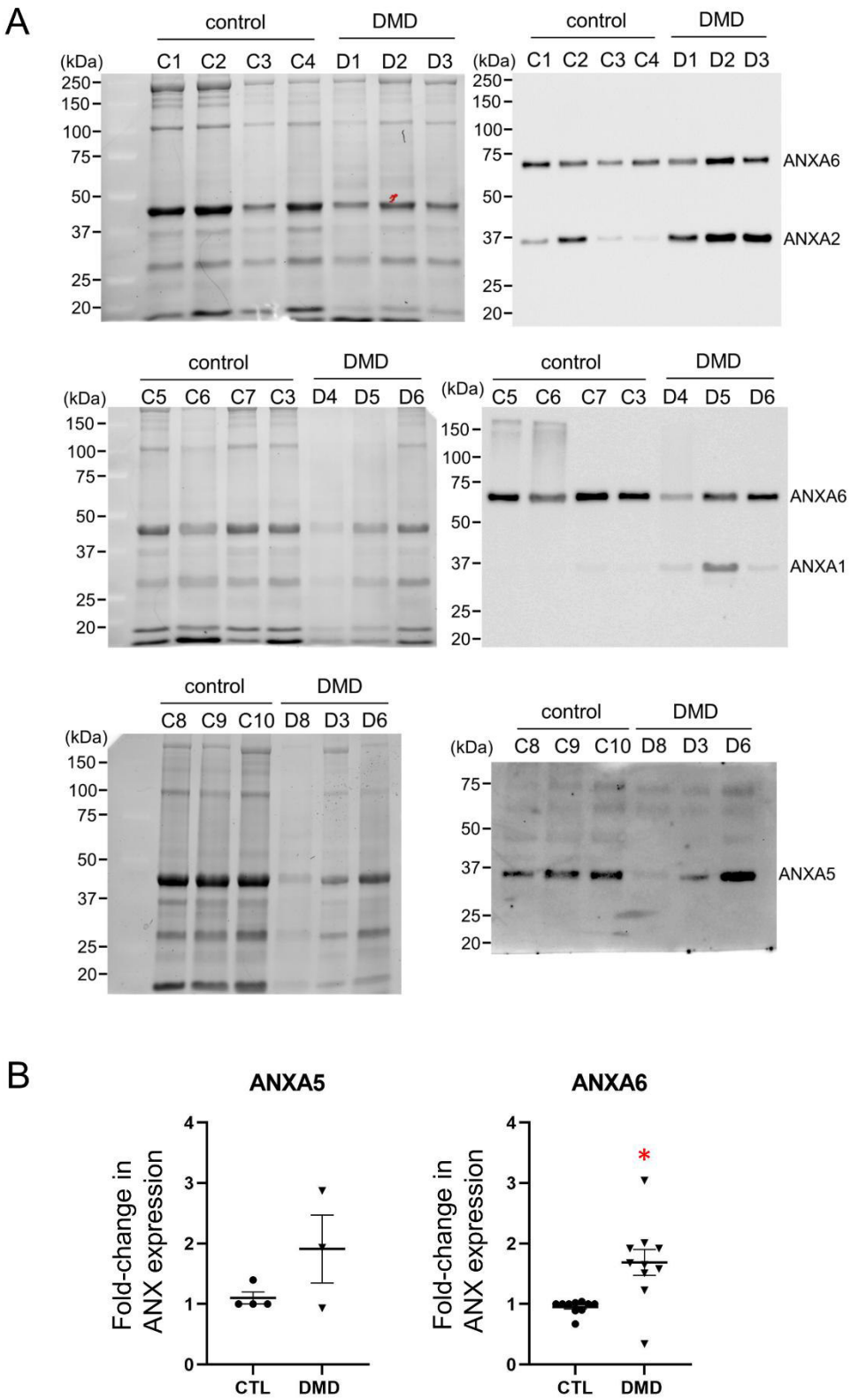

FIGURE S4 Annexin expression in control and DMD skeletal muscle biopsies. A) Annexin expression was quantified by western-blot analysis (right-hand images). Normalization was performed by total protein detection (left-hand images). Scatter plots displaying fold-change values in annexin expression between DMD and control samples are presented in Figure 3B. B) ANXA5 and ANXA6 plots presented in Figure 3B with the vertical axis scale adjusted to better highlight the differences. Wilcoxon signed rank test. *: $p < 0.05$.

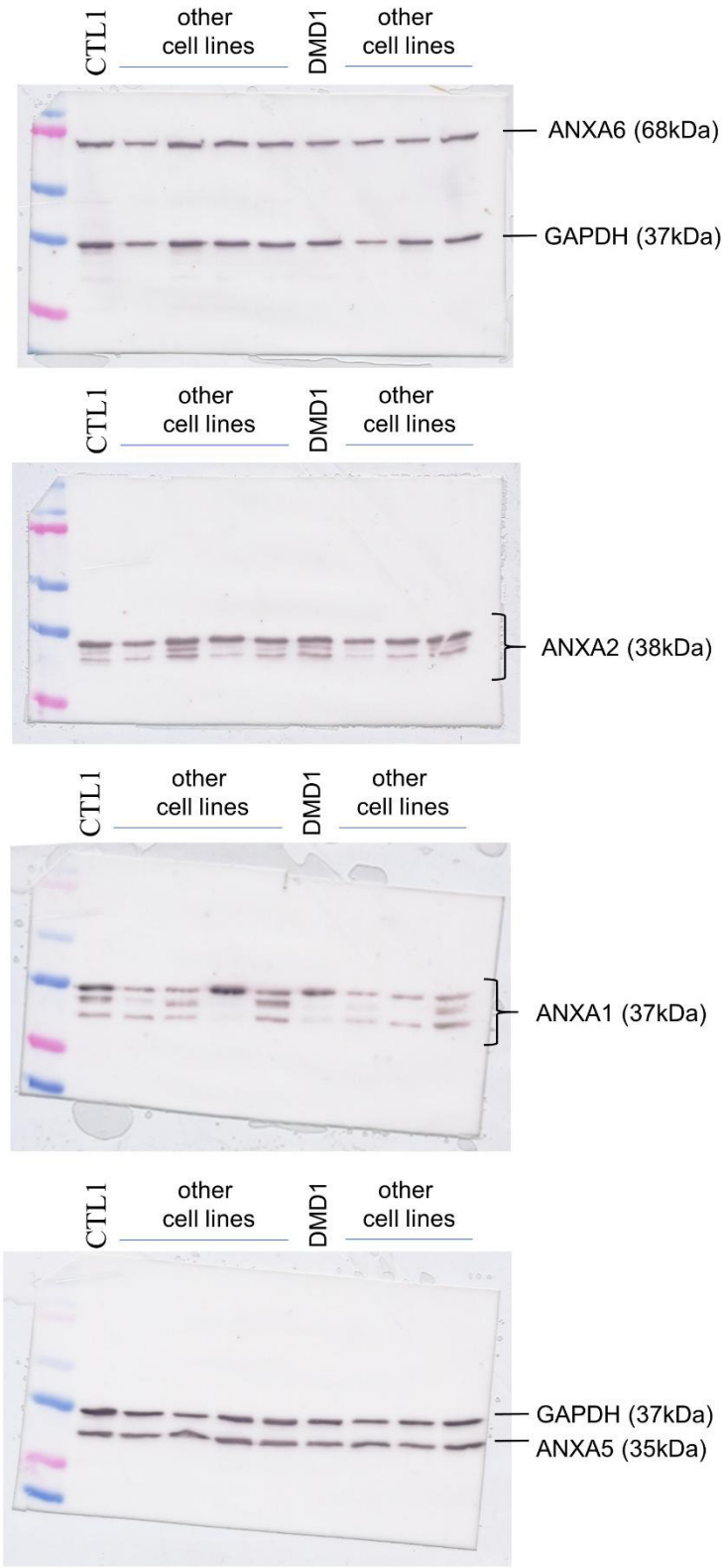

FIGURE S5 Annexin expression in control and DMD skeletal muscle cell lines. Annexin expression was quantified by western-blot analysis as described in the legend of Figure 4. As ANXA1 and ANXA2 molecular weights are similar to GAPDH, this loading control was immunodetected only on ANXA5 and ANXA6 membranes. Scatter plots displaying annexin relative expression are presented in Figure 4B.

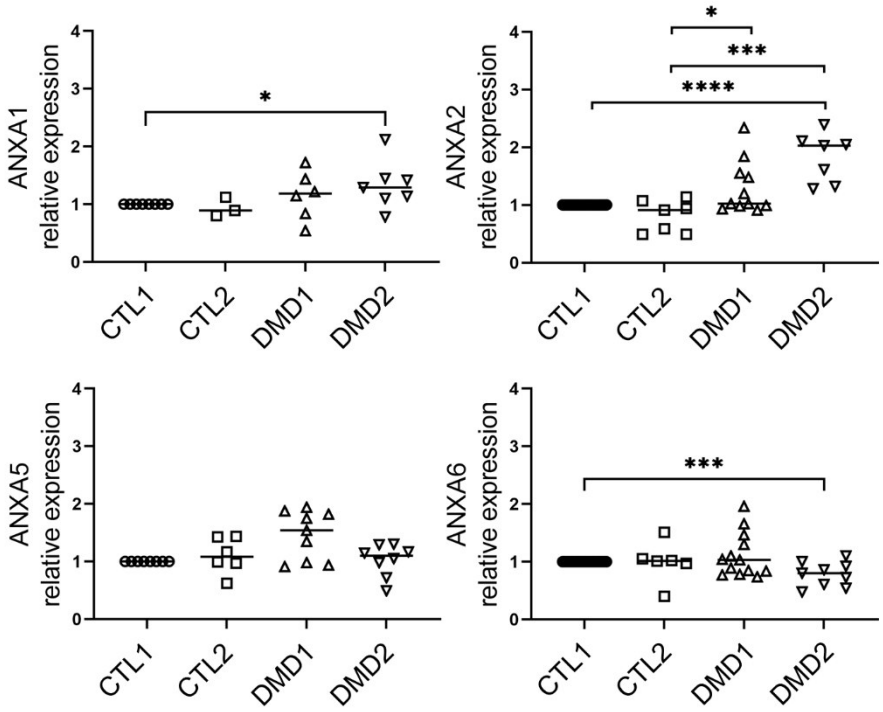

FIGURE S6 Annexin expression in control and DMD skeletal muscle cell lines. Annexin expression was quantified by western-blot analysis as described in the legend of Figure 4. These scatter plots present data obtained for each cell line. Wilcoxon signed rank test using CTL1 as a reference. *: $p < 0.05$; ***: $p < 0.001$; ****: $p < 0.0001$.

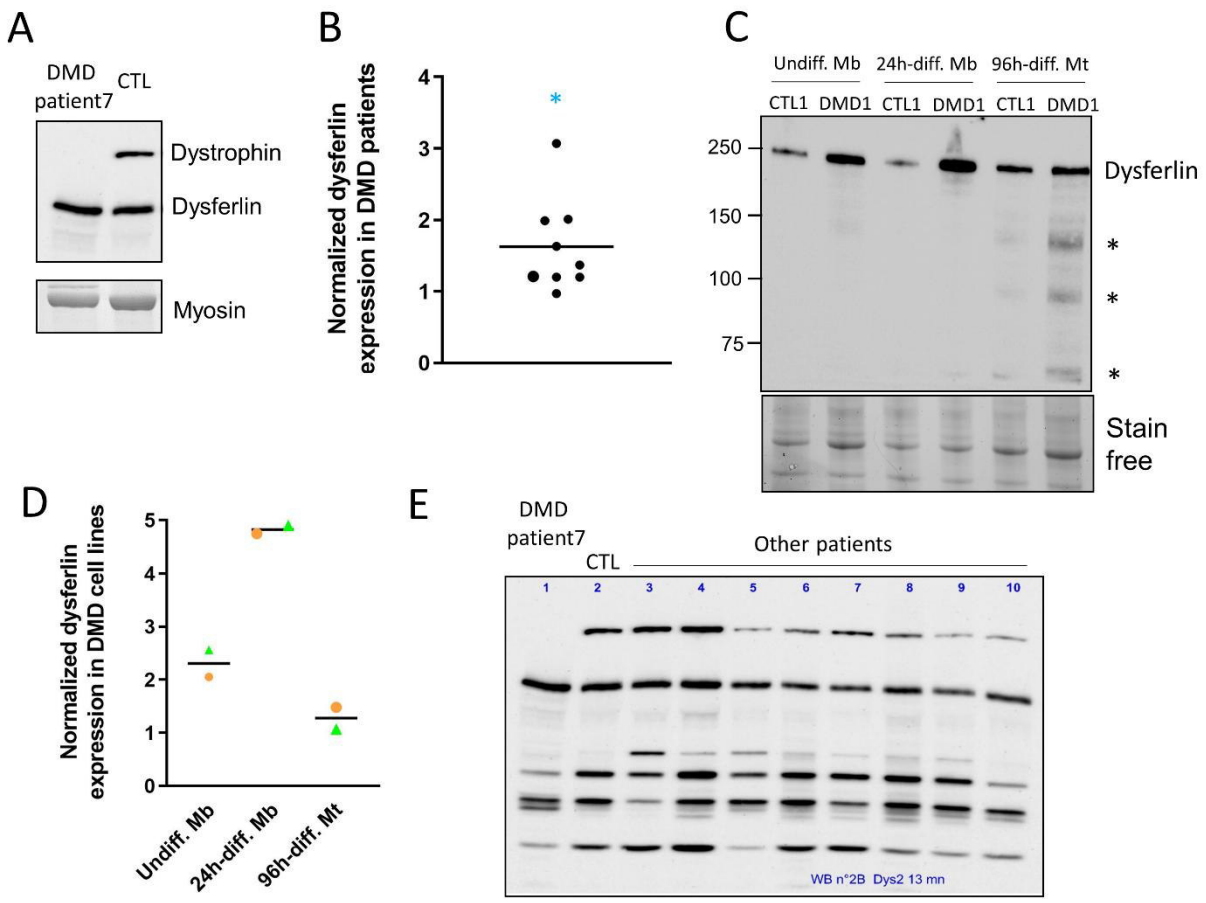

FIGURE S7 Dysferlin expression in control and DMD skeletal muscle cells and biopsies. A) Dysferlin expression was quantified by multiplexed western-blot analysis, as previously described (Anderson and Davison Am J Pathol. 1999 154(4):1017-22), in muscle biopsies of DMD patients and compared to control individual. The entire membrane is presented in E. B) The scatter plot presents expression of dysferlin in DMD patients (n = 9) normalized for myosin expression and relative to dysferlin expression in the control (n = 9). Data were analyzed with the One sample t test (theorical mean = 1, p-value = 0.0202, *). The mean and median values were 1.63 ± 0.65 and 1.37, respectively. These values, being significantly greater than 1, indicate that dysferlin expression is increased in DMD patients compared with controls. C) Dysferlin expression was quantified by Western blot in CTL1 and DMD1 cell lines as described in the legend of Figure S2 with minor modifications. A stain-free 7.5% acrylamide gel was used and the transfer time was 10 min rather than 15 min at 1.3 A/25 V. In the control CTL1 cell line, dysferlin signal increases during differentiation, as expected. A stronger signal is observed in the DMD1 cell line compared to CTL1. In the DMD1 myotubes (96h-diff. Mt), we observed a decrease in the signal corresponding to the full-length dysferlin compared to DMD1 myoblasts, accompanied by the appearance of truncated forms that may correspond to mini-dysferlin (*), notably the 72 kDa mini-dysferlin product previously described (Lek et al. J Neurosci. 2013 33(12):5085–5094). D) The scatter plot presents data obtained for DMD1 cell line relative to CTL1. Analysis was performed on undifferentiated myoblasts (Undiff. Mb), 24h-diferentiated myoblasts (24h-diff. Mb), and 96h-differentiated myotubes (96h-diff. Mt). E) The entire membrane from which has been extracted the blot presented in A. Duchenne muscular dystrophy was not diagnosed in the “other patients”.

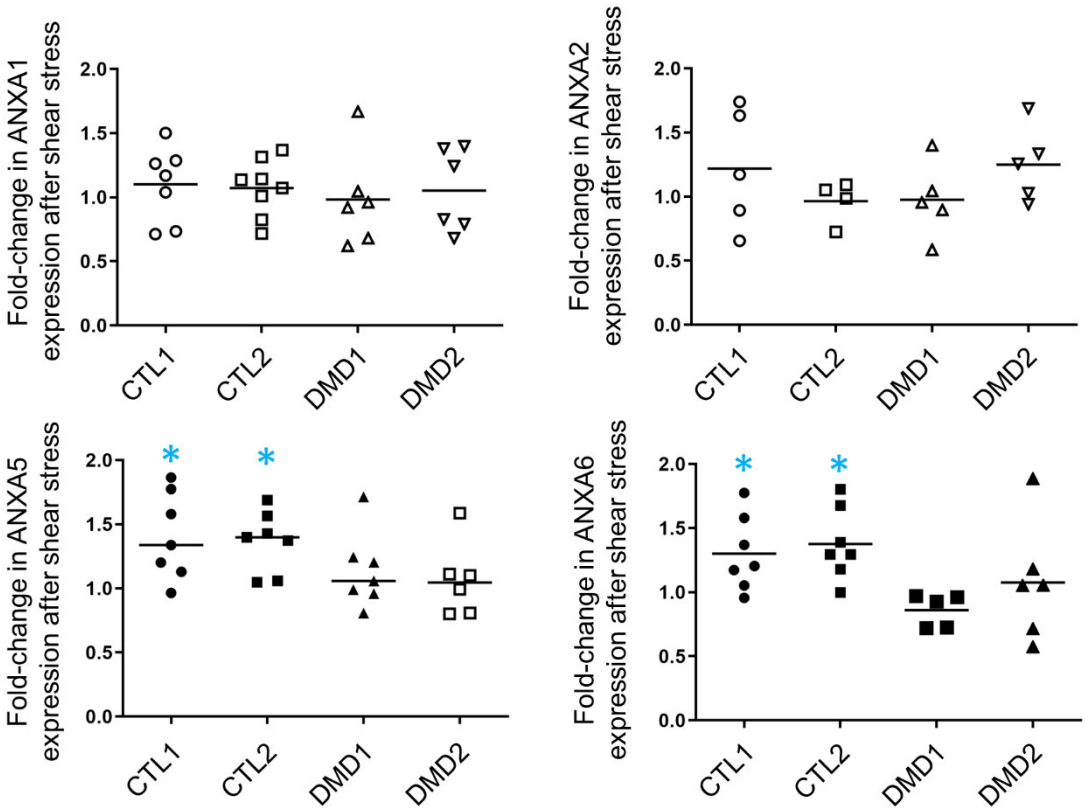

FIGURE S8 Annexin expression in control and DMD skeletal muscle cells submitted to shear stress. In addition to the data presented in Figure 5, scatter plots with mean value displaying the fold-change of annexin expression in each control and DMD skeletal muscle cell line after shear stress, normalized for the basal unstressed condition. Wilcoxon test. *: $p < 0.05$.

A

ANXA1 / laminin-α / Hoescht - control biopsy

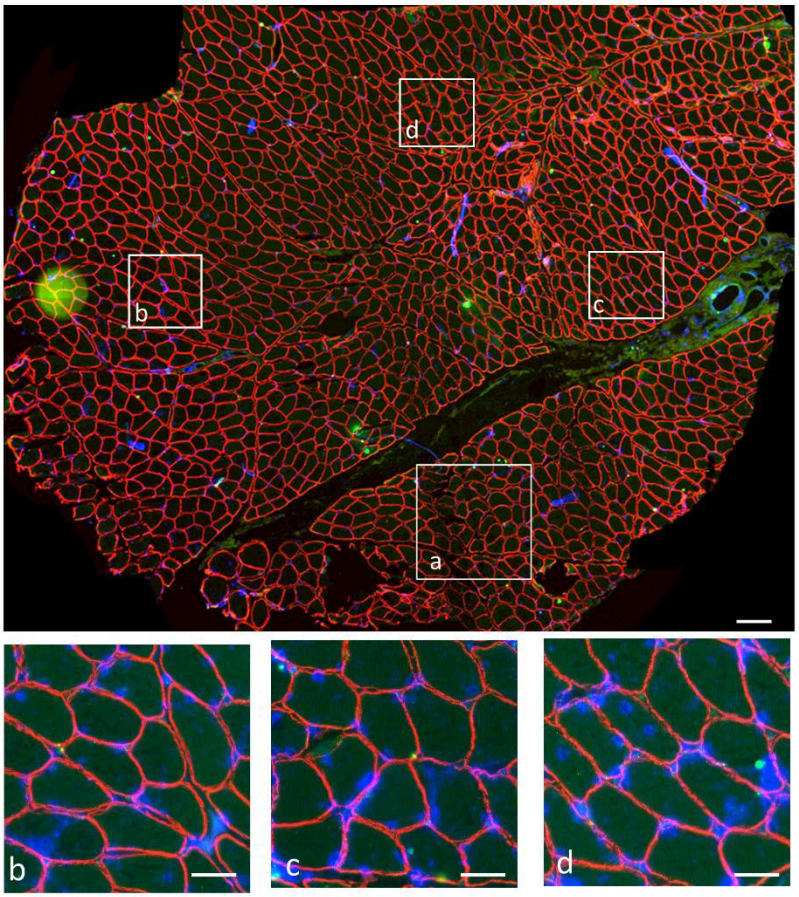

ANXA1 / laminin-α / Hoescht - DMD biopsy

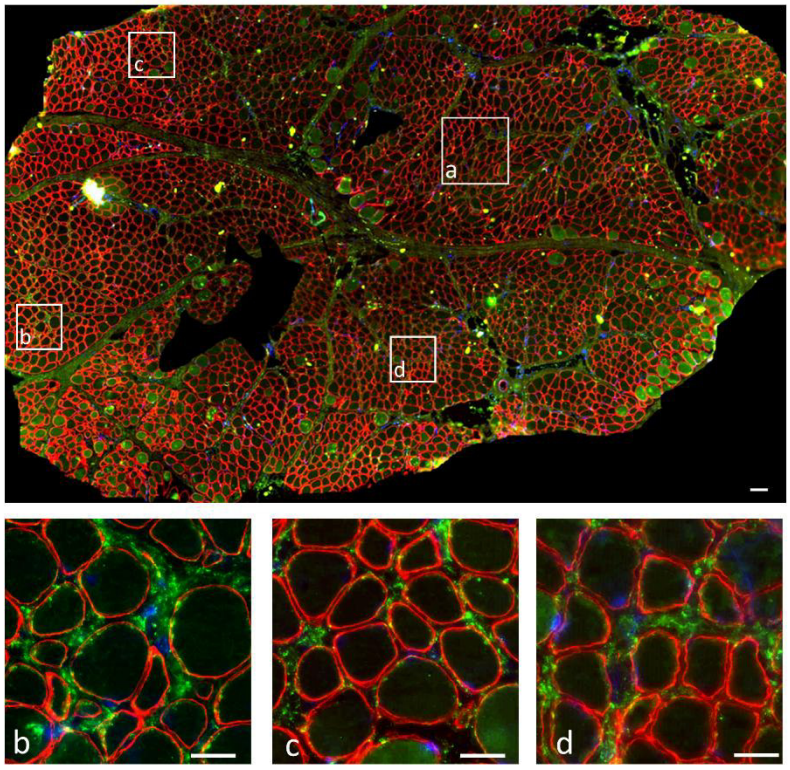

B

ANXA2 / laminin-α / Hoescht - control biopsy

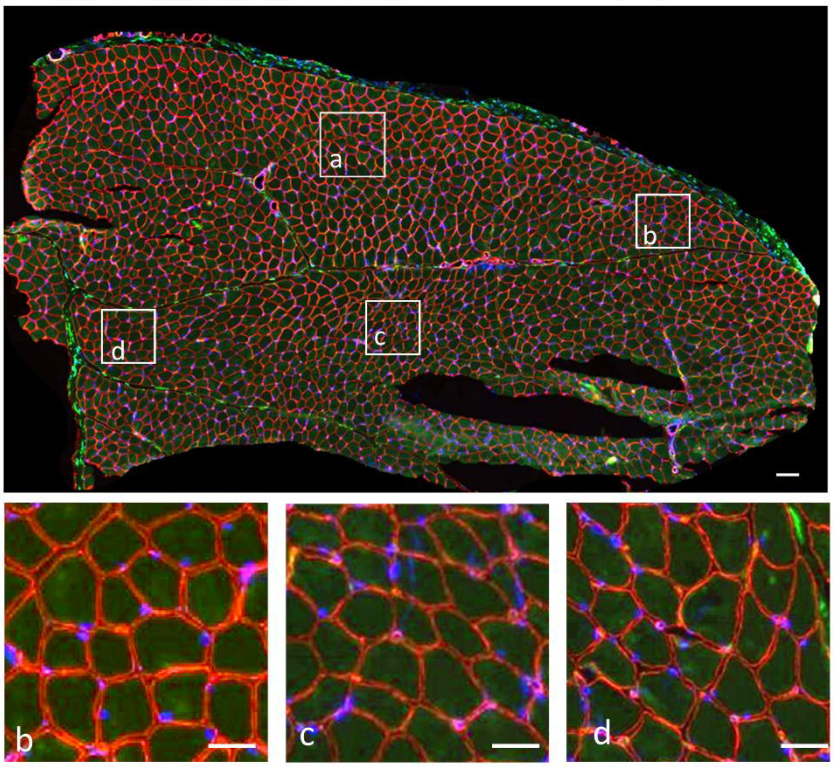

ANXA2 / laminin-α / Hoescht - DMD biopsy

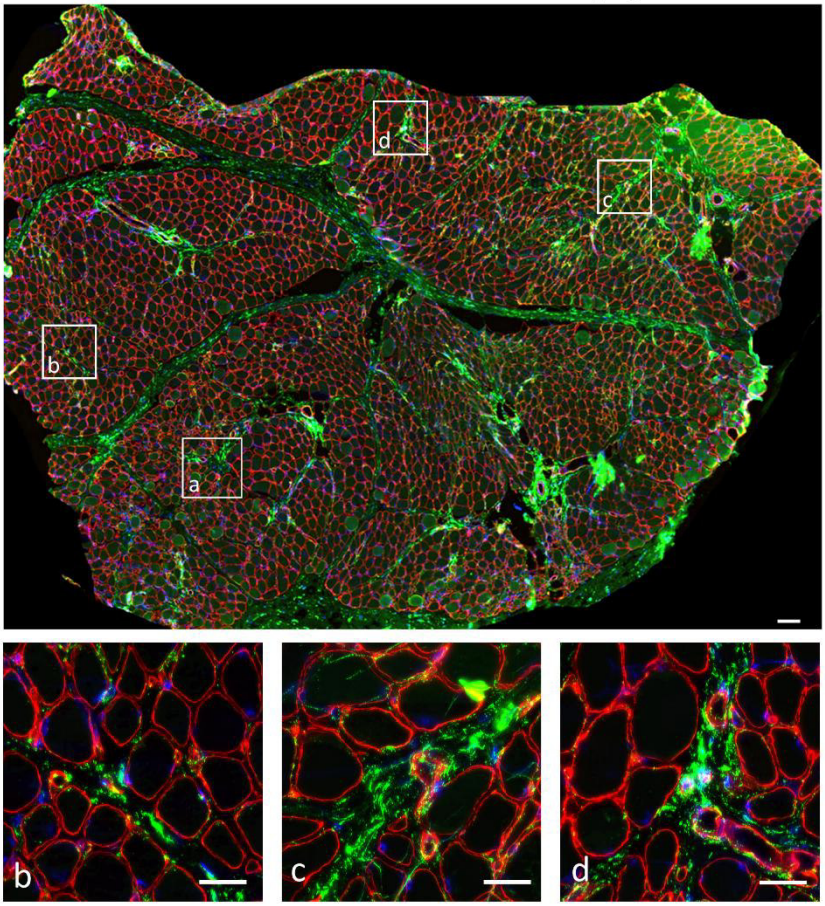

C

ANXA5 / laminin-α / DAPI - control biopsy

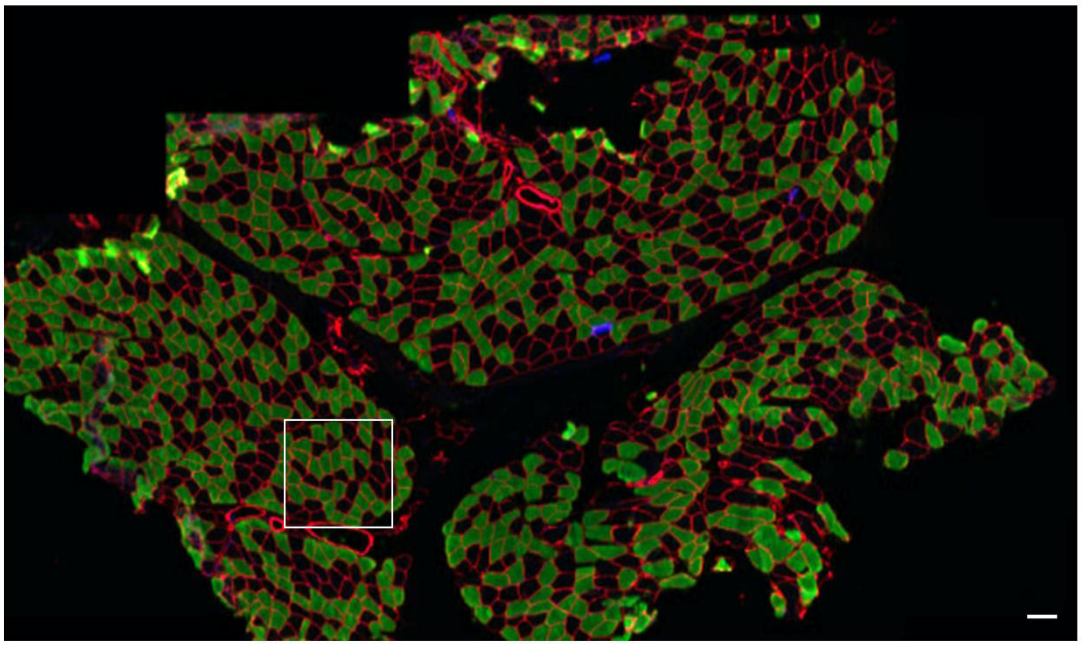

ANXA5 / laminin-α / DAPI - DMD biopsy

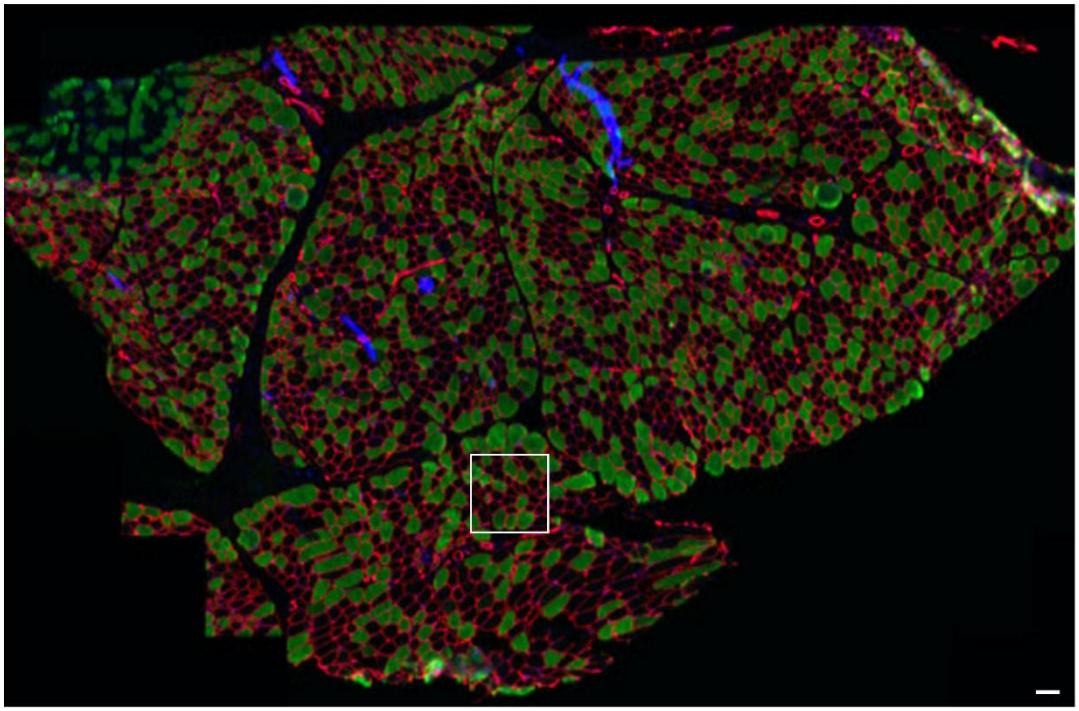

D

ANXA6 / laminin-α / DAPI - control biopsy

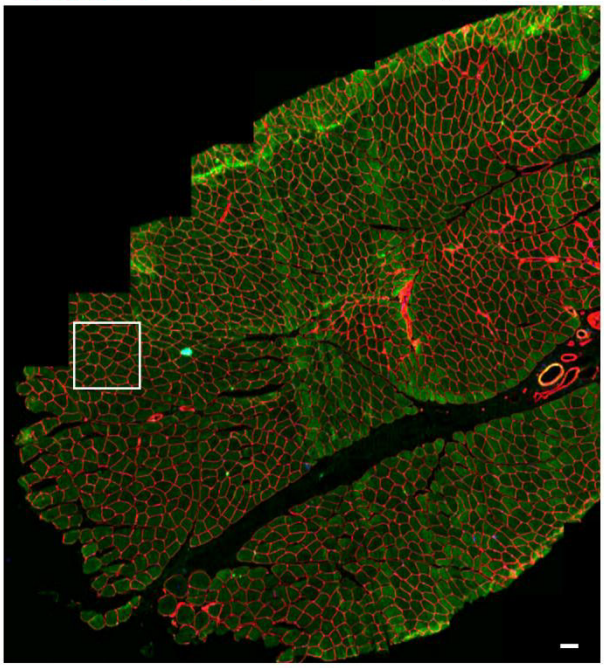

ANXA6 / laminin-α / DAPI - DMD biopsy

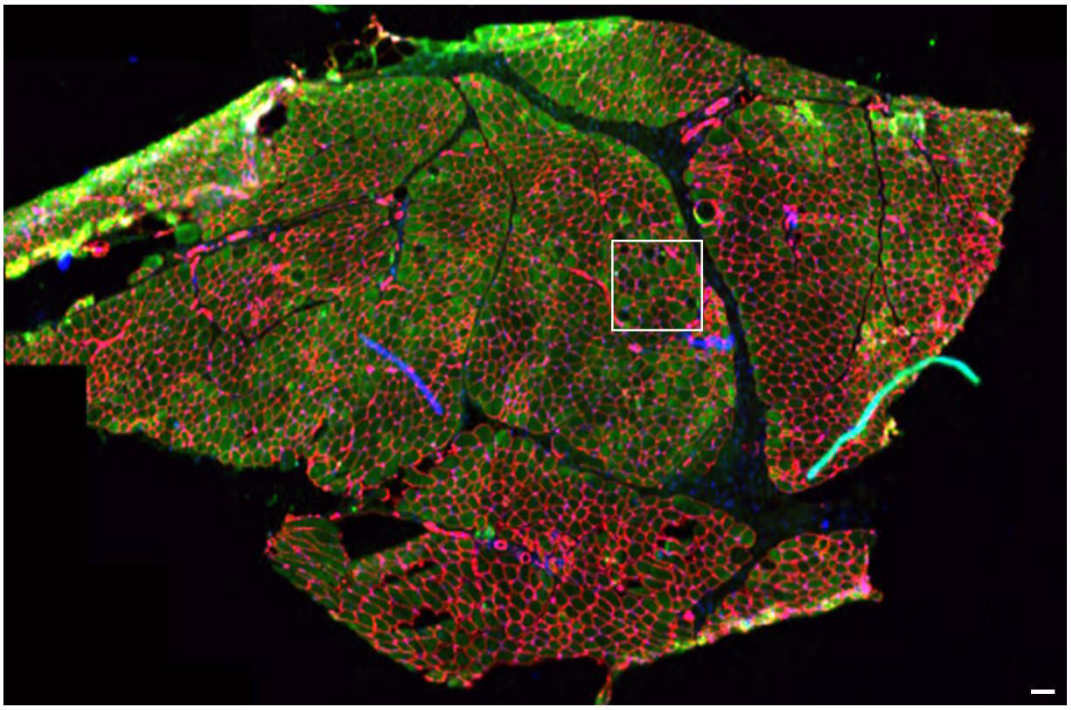

FIGURE S9 Whole-muscle section images including regions presented in Figure 6 for ANXA1 (A), ANXA2 (B), ANXA5 (C), and ANXA6 (D) immunostaining (green). Laminin-α (red) was also immunostained to detect sarcolemma. Nuclei were stained with DAPI (blue). White squares indicate regions presented at higher magnification. These regions are labeled from a to d; regions a are shown in Figure 6. Scale bars: 100 µm in whole-muscle sections; 50 µm in the magnified images.

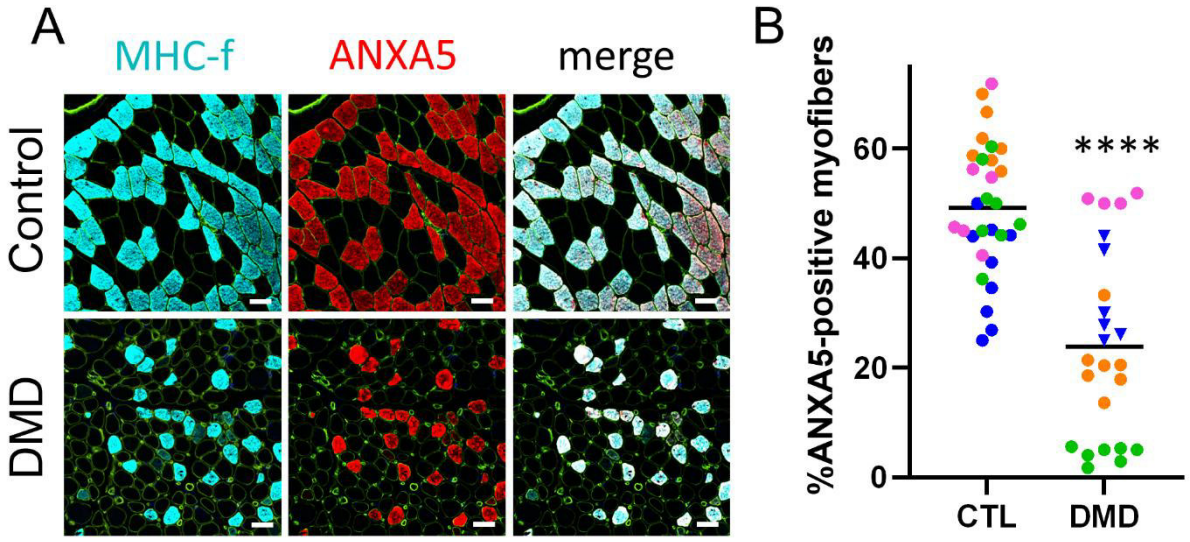

FIGURE S10 ANXA5 expression in control and DMD myofibers. A) Coimmunostaining of laminin-α (green), ANXA5 (red) and fast myosin heavy chain (MHC-f, blue) was performed to assess the specific presence of ANXA5 in type-II myofiber. B) Proportion of myofibers positive for ANXA5 was determined in control (n=4) and DMD (n=4) biopsies. Scatter plots with mean value displaying the percentage of ANXA5-positive myofibers. Each color corresponds to a control individual or a patient. Mann-Whitney test. ****$p < 0.0001$.

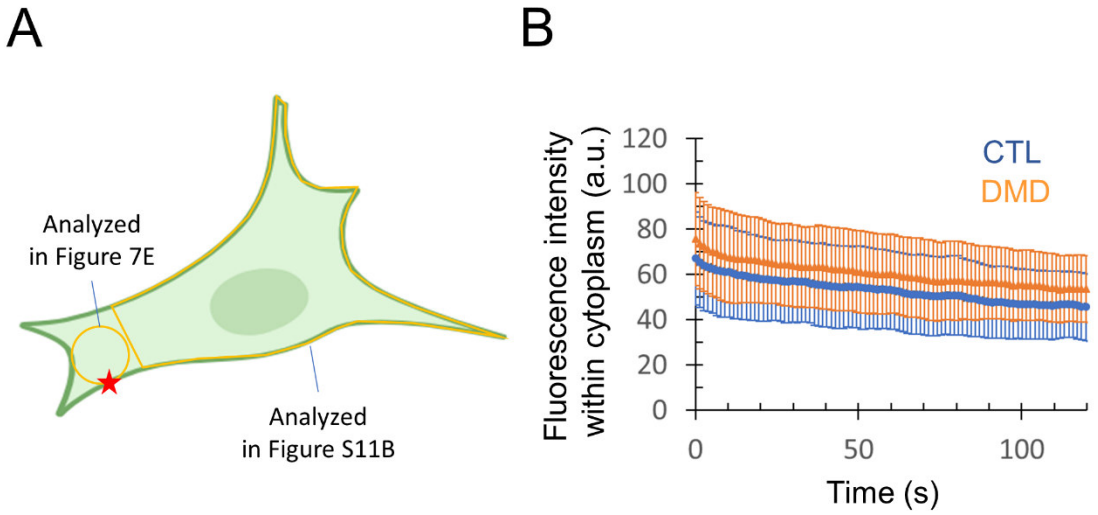

FIGURE S11 ANXA2 trafficking dynamics in control and DMD skeletal muscle cells following laser-induced membrane damage. A) Schematic illustrating the regions of interest (ROIs) used for quantifying ANXA2-GFP redistribution after injury. The circular ROI (yellow circle; 10 µm diameter; analyzed in Figure 7E) is centered at the disruption site (red star) to capture trafficking at the membrane lesion. A polygonal ROI (yellow shape; analyzed in Figure S11B) encompassing ~75% of the cell area - excluding the disruption site - is used to assess cytoplasmic trafficking. B) Time course of ANXA2-GFP fluorescence intensity within the cytoplasmic polygonal ROI for control (blue) and DMD (orange) myoblasts. Fluorescence intensity is expressed as mean ± SD (n = 6 cells per condition), reflecting intracellular trafficking dynamics in response to membrane injury.

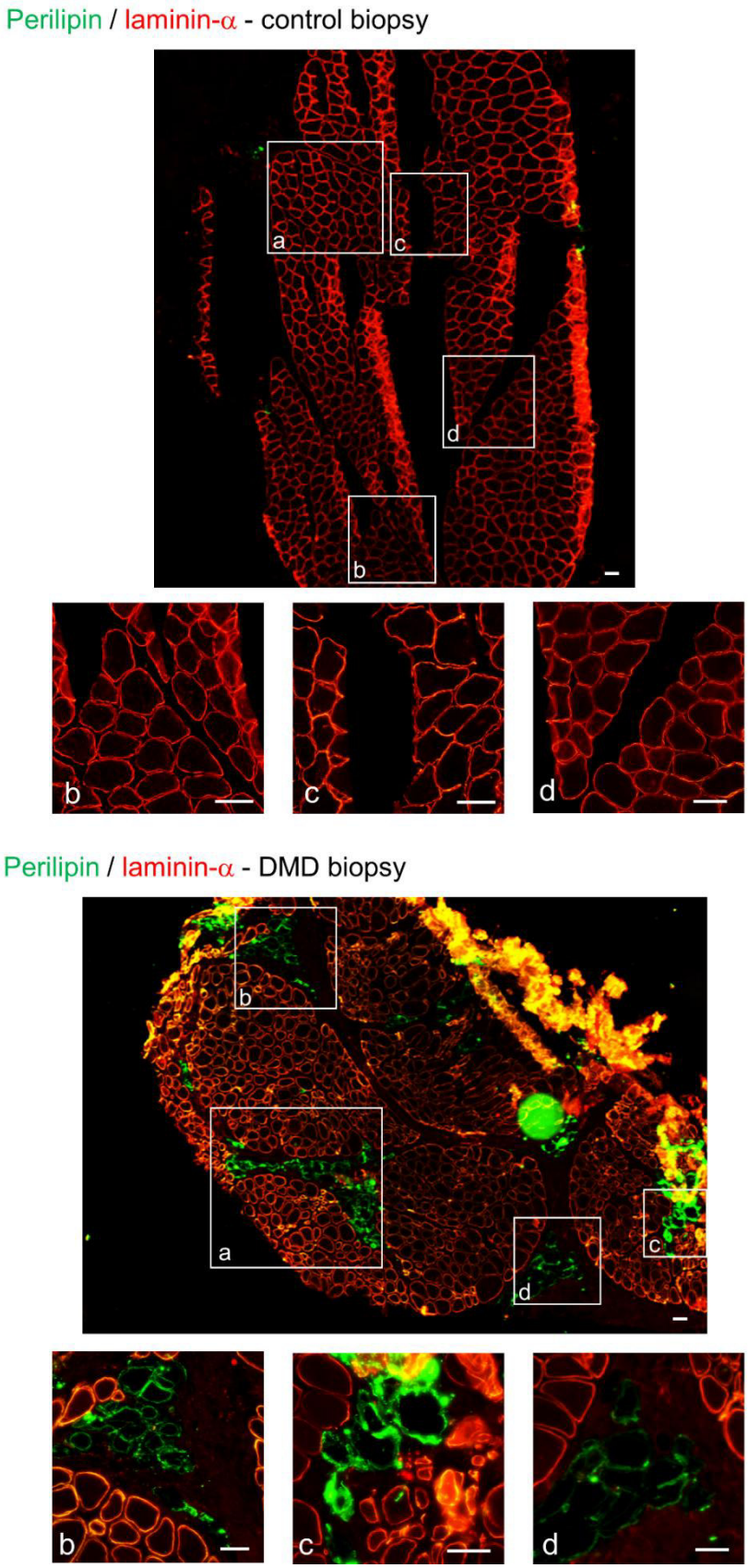

FIGURE S12 Control (upper panels) and DMD (lower panels) whole-muscle section images including regions presented in Figure 8 with perilipin (green) immunostaining to detect adipocytes and laminin-α (red) immunostaining to detect sarcolemma. White squares indicate the areas shown at higher magnification. These areas are labeled from a to d; regions a are shown in Figure 8.